Quarterly Technical Report 9 • 13 April 1995

IR MATERIALS PRODUCIBILITY

M.A. Berding, Sr. Research Physicist
A. Sher, Program Director
S. Krishnamurthy, Sr. Research Physicist
Physical Electronics Laboratory

SRI Project 3820

Prepared for:

Contracting Officer's Technical Representative
Advanced Research Projects Agency
Microelectronics Technology Office (MTO)
3701 N. Fairfax Drive
Arlington, VA 22203-1714

Attn: Mr. Raymond Balcerak

ARPA Order No. 8557; Program Code Nos. 2H20, 2D10

Contract MDA972-92-C-0053

Covering the period: 1 September through November 1994

IR MATERIALS PRODUCIBILITY

M.A. Berding, Sr. Research Physicist
A. Sher, Program Director
S. Krishnamurthy, Sr. Research Physicist
Physical Electronics Laboratory

SRI Project 3820

SRI Project 3820

Prepared for:

Contracting Officer's Technical Representative
Advanced Research Projects Agency
Microelectronics Technology Office (MTO)
3701 N. Fairfax Drive
Arlington, VA 22203-1714

Attn: Mr. Raymond Balcerak

ARPA Order No. 8557; Program Code Nos. 2H20, 2D10

Contract MDA972-92-C-0053

Covering the period: 1 September through November 1994

APPROVED FOR PUBLIC RELEASE
DISTRIBUTION UNLIMITED

Approved:

Eric Pearson, Director
Physical Electronics Laboratory

Donald L. Nielson, Vice President
Computing and Engineering Sciences Division

REPORT DOCUMENTATION PAGE

Form Approved
OMB No. 0704-0188

1. AGENCY USE ONLY (Leave Blank)	2. REPORT DATE	3. REPORT TYPE AND DATES COVERED
	13 April 1995	Quarterly Technical 9 (1 Sept. to Nov. 1994)

4. TITLE AND SUBTITLE

IR Materials Producibility

5. FUNDING NUMBERS

6. AUTHORS

M.A. Berding, A. Sher, S. Krishnamurthy

7. PERFORMING ORGANIZATION NAME(S) AND ADDRESS(ES)

SRI International
333 Ravenswood Avenue
Menlo Park, CA 94025-3493

8. PERFORMING ORGANIZATION REPORT NUMBER

9. SPONSORING/MONITORING AGENCY NAME(S) AND ADDRESS(ES

Advanced Research Projects Agency
Microelectronics Technology Office, Infrared Focal Plane Array Program
3701 North Fairfax Drive
Arlington, Virginia 22203-1714

10. SPONSORING/MONITORING AGENCY REPORT NUMBER

11. SUPPLEMENTARY NOTES

12a. DISTRIBUTION/AVAILABILITY STATEMENT

Approved for public release; distribution unlimited

12b. DISTRIBUTION CODE

13. ABSTRACT *(Maximum 200 words)*

The work summarized in this report covers the ninth quarter of a program with a goal that is threefold: first, to study the properties of native point defects in infrared focal-plane array (IRFPA) active and substrate materials; second, to study the properties of native point defects in two classes of photonic materials, the wide-gap II-VI compounds (ZnSe as the prototype for which impurity properties will also be calculated) and the nonlinear optical materials ($LiNbO_3$ as the prototype); the third, to study the properties of HgZnTe as a very-long-wave infrared (VLWIR) detector material. During the ninth quarter:

- Completed the calculation of the Hall coefficient in HgCdTe and related materials.
- Completed two papers for presentation at the MCT workshop.

14. SUBJECT TERMS

native point defects; infrared devices photonic material; HgTe; CdTe; ZnSe; HgCdTe

15. NUMBER OF PAGES

44

16. PRICE CODE

17. SECURITY CLASSIFICATION OF REPORT	18. SECURITY CLASSIFICATION OF THIS PAGE	19. SECURITY CLASSIFICATION OF ABSTRACT	20. LIMITATION OF ABSTRACT
Unclassified	Unclassified	Unclassified	Unlimited

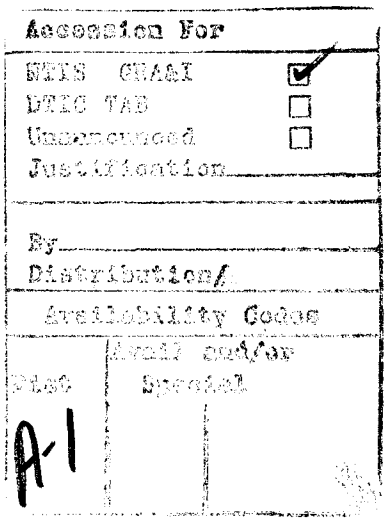

1. HALL COEFFICIENTS IN NARROWGAP SEMICONDUCTORS

We have completed our calculations of the Hall coefficients in HgCdTe and related materials. The Hall factor in small gap semiconductors is calculated by solving Boltzmann transport equation with full bandstructures and Fermi-Dirac statistics. Previous calculations based on relaxation time approximations indicated a large deviation in the Hall factor from unity. However, our detailed calculations yield a uniform value of unity for all temperatures at low carrier concentrations. Surprisingly, this is in agreement with the the value currently used in experiments which is based on parabolic approximation, Maxwell-Boltzmann distribution and relaxation time approximation. Further details of this work are given as Appendix A.

2. DEFECT MODELING STUDIES IN HgCdTe AND CdTe

An invited paper entitled "Defect modeling studies in HgCdTe and CdTe" was presented at the 1994 MCT Workshop in October. This paper is included as Appendix B.

We have speculated that the tellurium antisite is both the residual donor and a prinicpal contributor to Shockley-Reed recombination. Thus devising means to reducing the density of this defect is likely to improve devices. We have shown that the most likely diffusion path for the tellurium antisite is through a mercury vacancy assisted process. Therefore, to decrease the tellurium antisite concentrations one must first devise annealing strategies to accomplish this end prior to the low–temperature mercury–saturated anneal customairly used to elimate the mercury vacancy. A prescription to accomplish these goals has been formulated, and experiments to test its effectiveness are suggested.

Another major accomplishment reported on this period is a native point defect study of CdTe. Once again we agree with the limited experimental information available, and the details we present suggest means to imporve the material properties.

3. TEMPERATURE DEPENDENCE OF THE BAND GAPS IN HgCdTe AND OTHER SEMICONDUCTORS

A paper on the temperature dependence of the semiconductor band gaps was presented at the 1994 MCT Workshop. This paper is included as Appendix C.

APPENDIX A

Hall coefficients in narrow gap semiconductors

In the previous report we described our full-bandstructure calculation of Hall factor, r, as a function of impurity concentrations and temperature in the relaxation time approximation. The obtained results showed a considerable increase in r, with a maximum value of 1.3, is expected at low concentrations and high temperatures. These observations had a strong effect on experimentally deduced impurity or intrinsic carrier concentrations and carrier mobilities as the experimentalists use a value of 1 for r. In this period, we carried out the detailed calculation of r by obtaining full solution to Boltzmann transport equation (BTE) in the presence of both electric and magnetic fields. In all our calculations, accurately obtained hyperbolic bandstructure for the conduction band is used.

Several methods to solve the BTE with full bandstructures and Fermi-Dirac (FD) statistics are described in the literature. However, all of them are time consuming iterative schemes. We had recently extended our efficient eigenvalue approach to solve BTE with FD statistics and external electric field[1]. This method was shown to be fast and to accurately obtain the electron mobility curves for various impurity concentrations and temperatures. We further extend this method to include the effect of crossed magnetic field.

The steady state BTE in the presence of electric (**E**) and magnetic (**B**) fields is,

$$\nabla f(\mathbf{k}) \cdot \frac{e}{\hbar}(\mathbf{E} + \mathbf{v} \times \mathbf{B}) = \sum_{\mathbf{k}'} [w(\mathbf{k},\mathbf{k}')f(\mathbf{k}')(1 - f(\mathbf{k})) - w(\mathbf{k}',\mathbf{k})f(\mathbf{k})(1 - f(\mathbf{k}'))] \quad (1)$$

The first term of the right hand side is the gain term and the second one is the loss term. In equilibrium, the left hand side of Eq.(1) is identically zero and because, in general for a system of interest interacting with a heat bath $w(\mathbf{k},\mathbf{k}')\, e^{-\beta E_{\mathbf{k}'}} = w(\mathbf{k}',\mathbf{k})\, e^{-\beta E_{\mathbf{k}}}$, f becomes the equilibrium FD distribution function f_0 given by,

$$f_{00}(E_k) = \left(e^{\frac{(E_k - \epsilon_F)}{k_B T}} + 1\right)^{-1} \quad (2)$$

where ϵ_F is the Fermi energy. The solution $f(\mathbf{k})$ can always be written as a sum of $f_{00}(\mathbf{k})$ and some deviation, $\Delta(\mathbf{k})$. That is,

$$f(\mathbf{k}) = f_{00}(\mathbf{k}) + \Delta(\mathbf{k}) \quad (3)$$

Note that $\sum_{\mathbf{k}} \Delta(\mathbf{k})$ is zero for a sample with ohmic contacts because the number of electrons should remain constant. Combining Eq.(1) through Eq.(3), we get,

$$\nabla f(\mathbf{k}) \cdot \frac{e}{\hbar}(\mathbf{E} + \mathbf{v} \times \mathbf{B}) = \sum_{\mathbf{k}'} [W(\mathbf{k},\mathbf{k}')\Delta(\mathbf{k}') - W(\mathbf{k}',\mathbf{k})\Delta(\mathbf{k}) + (w(\mathbf{k}',\mathbf{k}) - w(\mathbf{k},\mathbf{k}'))\Delta(\mathbf{k})\Delta(\mathbf{k}')] \quad (4)$$

where the renormalized W and the usual transition probability per unit time w are related by,

$$W(\mathbf{k},\mathbf{k}') = w(\mathbf{k},\mathbf{k}')\frac{(1-f_{00}(\mathbf{k}))}{(1-f_{00}(\mathbf{k}'))} \tag{5}$$

Note that for elastic scattering W and w are equal. However, for inelastic cases the relative size of W to w depends on whether energies at k and k' are larger or smaller than ϵ_F . If both initial and final energies are larger (or smaller) than ϵ_F , then only small corrections to w occur. However, if the initial state is above ϵ_F and the final state is below ϵ_F , then for that scattering event W is suppressed. This tends, for example, to decrease the contribution of inelastic scattering events involving phonon emission. Also notice that in the event the perturbation is small, then the Δ^2 term can be neglected and Eq.(4) resembles the traditional MB steady state BTE where W plays the role of w.

We further expand $\Delta(\mathrm{k})$ in power series of an indexing parameter λ and β, which we will eventually set to unity. Thus,

$$\Delta(k) = \sum_{n,m=1}^{\infty} f_{nm}(\mathbf{k})\lambda^n\beta^m \tag{6}$$

Substituting Eq.(6) in Eq.(4) and noting that f(k) has one additional term, we get,

$$\begin{aligned}\sum_{n,m=0}^{\infty} \nabla f_{nm}(\mathbf{k})\cdot\frac{e}{\hbar}(\mathbf{E}+\mathbf{v}\times\mathbf{B})\lambda^n\beta^m = \\ \sum_{\mathbf{k}',n,m=1}^{\infty}\left[W(\mathbf{k},\mathbf{k}')f_{nm}(\mathbf{k}') - W(\mathbf{k}',\mathbf{k})f_{nm}(\mathbf{k})\right]\lambda^n\beta^m \\ + \sum_{\mathbf{k}';n,m,n',m'=1}^{\infty}\left[w(\mathbf{k}',\mathbf{k}) - w(\mathbf{k},\mathbf{k}')\right]f_{nm}(\mathbf{k})f_{n'm'}(\mathbf{k}')\lambda^{n+n'}\beta^{m+m'}\end{aligned} \tag{7}$$

Noting that the indices λ and β are proportional to $\mathbf{E}$ and $\mathbf{B}$ respectively, we can collect the coefficients of the same power of λ and β on both sides to get a series of equations. However, for our purpose of calculating r where only small fields are applied, we consider only $\lambda^1\beta^0$, $\lambda^0\beta^1$, and $\lambda^1\beta^1$ terms. We get,

$$\nabla f_{00}(\mathbf{k})\cdot\frac{e}{\hbar}\mathbf{E} = \sum_{\mathbf{k}'}\left[W(\mathbf{k},\mathbf{k}')f_{10}(\mathbf{k}') - W(\mathbf{k}',\mathbf{k})f_{10}(\mathbf{k})\right] \tag{8a}$$

$$\nabla f_{00}(\mathbf{k})\cdot\frac{e}{\hbar}(\mathbf{v}\times\mathbf{B}) = \sum_{\mathbf{k}'}\left[W(\mathbf{k},\mathbf{k}')f_{01}(\mathbf{k}') - W(\mathbf{k}',\mathbf{k})f_{01}(\mathbf{k})\right] \tag{8b}$$

and

$$\nabla f_{10}(\mathbf{k}) \cdot \frac{e}{\hbar}(\mathbf{v} \times \mathbf{B}) = \sum_{\mathbf{k}'} [W(\mathbf{k},\mathbf{k}') f_{11}(\mathbf{k}') - W(\mathbf{k}',\mathbf{k}) f_{11}(\mathbf{k})] \tag{8c}$$

In the isotropic case that we study $\nabla f_{00}(\mathbf{k})$ and **v**are proportional to **k**and hence from Eq.(8b) f_{01} is identically zero. Note that this information is used in obtaining Eq.(8c). Knowing f_{00} (from Eq.(2)), Eq.(8a) is solved for f_{10} and the solution is used Eq.(8c) for f_{11}. This procedure can be continued to the required precision. We emphasize that for low field electric fields, only the lowest order equations given here need to be solved to obtain accurate answers. When hot electron effects are addressed, iterative solutions should be used.

As shown in previous publication (Krishnamurthy and Sher, J. Appl. Phys., **75**, 7904 (1994)), Eqs.(8a) and (8c) are efficiently solved in a matrix inversion method by expanding the distribution functions in terms a finite set of basis functions. Once the functions f_{10} and f_{11} are obtained, the drift velocity, v_d, drift mobility, μ_d, Hall coefficient, R and Hall factor, r are easily calculated. We assume that **E** is in z direction and **B** is in y direction.

$$R = \frac{E_y}{j_E B}$$
$$= \frac{1}{ne} r$$

$$E_y = \frac{j_B}{\sigma}$$
$$\sigma = ne\mu_E$$
$$j_E = nev_d^E$$
$$j_B = nev_d^B$$

$$v_d^E = \frac{\sum_{\mathbf{k}} v_{\mathbf{k}} f_{10}(\mathbf{k})}{\sum_{\mathbf{k}'} f_{00}(\mathbf{k}')}$$
$$v_d^B = \frac{\sum_{\mathbf{k}} v_{\mathbf{k}} f_{11}(\mathbf{k})}{\sum_{\mathbf{k}'} f_{00}(\mathbf{k}')}$$

$$\mu_E = \frac{v_d^E}{E}$$

All of the above equations can be combined to yield a final expression,

$$r = \frac{v_d^B}{\mu_E v_d^E B}$$

We calculated the Hall factor, r for GaAs and $Hg_{0.78}Cd_{0.22}Te$ alloy as a function of temperature and impurity concentrations. Interestingly, the calculated values at low carrier concentrations are always around 1 for any temperature. While the final result comfortably justifies the value currently used by experimentalists, it should be noted that physics is quite different. The value of 1 for r is obtained with parabolic bandstructures, Maxwell-Boltzmann distribution and relaxation time approximation. We had shown that all these approximations are incorrect for small gap semiconductors like HgCdTe. While the removal of approximations correct the mobilities, Fermi energy and temperature dependent band gap substantially, the Hall factor remain unaffected.

We are in the process of calculating Hall factor for high dopant concentrations.

APPENDIX B

Defect modeling studies in HgCdTe and CdTe

DEFECT MODELING STUDIES IN HgCdTe and CdTe

M. A. BERDING, A. SHER, and M. VAN SCHILFGAARDE
SRI International, Menlo Park, California 94025

ABSTRACT

We have used a quasichemical formalism to calculate the native point defect densities in $x = 0.22$ $Hg_{1-x}Cd_xTe$ and CdTe. The linearized muffin–tin orbital method, based on the local density approximation and including gradient corrections, has been used to calculate the electronic contribution to the defect reaction free energies, and a valence force field model has been used to calculate the changes to the vibration free energy when a defect is created. We find the double acceptor mercury vacancy is the dominant defect, in agreement with previous interpretations of experiments. The tellurium antisite, which is a donor, is also found to be an important defect in this material. The mercury vacancy tellurium antisite pair is predicted to be well bound, and is expected to be important for tellurium antisite diffusion. We consider the possibilities that the tellurium antisite is the residual donor and a Shockley–Read recombination center in HgCdTe, and suggestions for further experimental work are made. We predict that the cadmium interstitial, a double acceptor, is the dominant defect for low cadmium pressures, while the cadmium interstitial, a double donor, dominates at high cadmium pressures.

Key words: HgCdTe, CdTe, defects, defect complexes

INTRODUCTION

The pseudobinary semiconductor alloy $Hg_{1-x}Cd_xTe$ with x=0.22 is currently the material of choice for high–performance detectors in the long–wavelength infrared (LWIR) (8–14 μm). Unlike most other II–VI systems, both extrinsic p– and n–type doping can be achieved in HgCdTe, although in as–grown material the electrical characteristics are often determined by native point defect concentrations. Understanding the properties of point defects and manipulation of their densities during growth and processing is essential to high–yield manufacturing of focal plane arrays (FPAs). As in other semiconductors, it is difficult to establish the presence and identity of all the important neutral and compensating point defects during growth and processing, much less to determine their concentrations. CdTe is important both as a substrate and passivating material for epitaxial layers of LWIR HgCdTe. Native point defects are of interest in CdTe in that they relate to its stoichiometry (which in turn has been shown to impact the minority carrier lifetimes[1] in HgCdTe devices), the formation and annihilation of tellurium precipitates,[2] and the self– and inter–diffusion coefficients that impact materials stability during growth, during subsequent processing, and over the device lifetime.

Our goal in this paper is to theoretically identify the important native defects in HgCdTe and CdTe, to calculate their densities as a function of growth and processing conditions, to validate our predictions by comparison with experimentally deduced properties of the native defects, and to suggest new experiments to begin to unravel the remaining mysteries in these materials. We have included in our analysis of HgCdTe both neutral and ionized states of eight native point defects and one defect pair. Our focus is on $x = 0.2$ (for comparison to annealing data[3]), $x = 0.22$ (for LWIR applications), and $x = 1$ (for substrate and passivating layers) $Hg_{1-x}Cd_xTe$. Our analysis of CdTe includes eight neutral native point defects. As we will show, we have attempted to incorporate all of the important contributions to the defect formation free energies and adopt a first–principles

approach for most of the quantities we calculate.

METHODOLOGY

To calculate the concentration of the native point defects in HgCdTe we employ a quasichemical formalism[4] in which the formation of independent crystalline defects is expressed as chemical reactions. For example, for the formation of the neutral mercury vacancy in HgTe with the mercury vapor as the reference phase, we have the reaction

$$\mathrm{HgTe} \rightarrow V_{\mathrm{Hg}}^{\times}\mathrm{Te} + \mathrm{Hg}_{vapor}. \tag{1}$$

Our notation is that of Kröger[4] in which the primary symbol is the defect species and the subscript indicates the site the defect occupies; V indicates the vacancy, and I the interstitial, and no subscript indicates the species is occupying its normal lattice position; $\times$ indicates the neutral defect species. Although we have chosen the mercury in the vapor phase as our reference and thereby will choose a mercury pressure to determine the chemical potential of mercury in the system, one could have chosen some other reference state for the mercury or tellurium (for example, by specifying a binary solution of $\mathrm{Hg}_{1-y}\mathrm{Te}_y$ at some temperature T in coexistence with the HgTe solid, as is essentially done during liquid phase epitaxy (LPE) growth). For our equilibrium calculations, the limits of mercury pressures within the existence region of $\mathrm{Hg}_{1-x}\mathrm{Cd}_x\mathrm{Te}$ are taken from experiment.[5]

In a similar manner, reactions can be written for the other point defects of the system. In our analysis we have included eight native point defects (plus their ionized species and the electron and hole): the mercury and tellurium vacancies (V_{Hg} and V_{Te}), the mercury and tellurium antisites ($\mathrm{Hg}_{\mathrm{Te}}$ and $\mathrm{Te}_{\mathrm{Hg}}$, and two types of mercury and tellurium tetrahedral interstitials—one surrounded by four cation near–neighbors ($\mathrm{Hg}_{I_{\mathrm{Hg}}}$ and $\mathrm{Te}_{I_{\mathrm{Hg}}}$) and the other surrounded by four anion near–neighbors ($\mathrm{Hg}_{I_{\mathrm{Te}}}$ and $\mathrm{Te}_{I_{\mathrm{Te}}}$). We have also included the bound mercury vacancy tellurium antisite pair $(V_{\mathrm{Hg}} - \mathrm{Te}_{\mathrm{Hg}})_{pair}$, in which the vacancy and antisite occupy near–neighbor cations sites, via the reaction

$$V_{\mathrm{Hg}} + \mathrm{Te}_{\mathrm{Hg}} \rightarrow (V_{\mathrm{Hg}} + \mathrm{Te}_{\mathrm{Hg}})_{pair}. \tag{2}$$

For low densities of noninteracting defects, the law of mass action can be used to determine the neutral defect concentrations. For the mercury vacancy this corresponds to

$$K_{V_{\mathrm{Hg}}^{\times}} \equiv \theta \exp\left(-\frac{F_{V_{\mathrm{Hg}}^{\times}}}{k_B T}\right) = [V_{\mathrm{Hg}}^{\times}] \tag{3}$$

where $F_{V_{\mathrm{Hg}}^{\times}}$ is the reaction free energy for the neutral mercury vacancy, k_B is Boltzmann's constant, T is the temperature in kelvin, and θ is the number of unit cells per unit volume. Thus, once the reaction free energy is known, it is straightforward to calculate the defect concentrations. Of course, all the work is involved in the calculation of the reaction free energies.

We have attempted to calculate all of the important contributions to the defect reaction free energies. An electronic contribution to the free energy results from the change in the total electron energy of the solid when a neutral defect is created; included in this energy is the electronic energy of free mercury atoms generated or consumed in the defect reaction. To calculate the electronic contribution we employ the self–consistent

first–principles full–potential linearized muffin–tin orbital method[6] and the local–density approximation (LDA), including gradient corrections of the Langreth–Mehl–Hu type[7] (which greatly improves the overbinding found in the LDA[8,9]). The vibrational modes of the system are also changed when a defect is created; we calculate this change to the formation free energy (both the enthalpy and entropy) using a Green's function formalism within a valence force model plus point–charge ionic model. An entropy contribution to the formation free energy also arises from the partial occupation of degenerate levels associated with the defect and from the introduction of a preferred direction via a symmetry–lowering Jahn–Teller distortion.[10] The combination of the electronic, vibrational, degeneracy, and translational (for the calculation of the chemical potential of the mercury atom in the vapor phase) free energies encompasses the primary contributions to the total defect formation free energies when referenced to a mercury vapor. Details of the results for these energies are given in Ref. 9. We have completed only preliminary calculations for the binding energy of the mercury vacancy tellurium antisite pair indicated in Eq. 3, using a 32–atom supercell and with overall lattice constant relaxation only. We expect that this defect may show further relaxation, which could lower the defect pair binding energy and therefore increase their density.

Although we are interested in studying the properties of point defects in HgCdTe, the neutral defect reaction free energies are calculated for HgTe; because we predict that the defects with highest concentrations (the mercury vacancy and the tellurium antisite) reside on the cation sublattice and therefore have four tellurium atoms for first nearest neighbors, we expect that the presence of cadmium will introduce a minor modification to the formation free energies, and of the order of other approximations made in the calculation (for example, using supercells). The presence of cadmium may have a larger impact on interstitial formation free energies, which can occupy sites with cations as near–neighbors. Although we find the density of interstitials to be relatively low,[9] the cation interstitial in particular is very important in annealing of HgCdTe.[12] For the present we have included the effects of the cadmium only by adjusting the number of sites available for mercury vacancies and in calculating of the band structure used in predicting the ionized point defect concentrations. For further discussion and details of the calculation of the reaction free energies, see Ref. 9.

Because the native point defects will in general have localized levels in the band gap, we need to calculate the concentration of the ionized defects in addition to the neutral defects discussed above. Once the density of the neutral defects is determined, the concentration of ionized defects can be calculated from

$$\frac{[X']}{[X^\times]} = \frac{g_{X'}}{g_{X^\times}} \exp\left(\frac{\mu_F - E_a}{k_B T}\right) \tag{4}$$

for an acceptor defect X and

$$\frac{[Y^\bullet]}{[Y^\times]} = \frac{g_{Y^\bullet}}{g_{Y^\times}} \exp\left(\frac{E_d - \mu_F}{k_B T}\right) \tag{5}$$

for a donor defect Y. Once again we have adopted the notation of Kröger: the bullet superscript indicates a positive charge and a prime a negative charge. E_a and E_d are the one–electron acceptor and donor levels; μ_F is the Fermi energy, which is determined by demanding charge neutrality; and g_X is the degeneracy of the state, including both spin and Jahn–Teller[10] splitting. Generalizations of these expressions are used for multiply ionized defects. The calculation of the electron and hole populations demands a knowledge of the temperature–dependent band structure and use of Fermi–Dirac statistics. The only

significant empirical data we employ in this calculation are those needed to obtain the temperature–dependent band structure, which is extrapolated to high temperatures at which equilibration and annealing take place and for which we are going to predict defect concentrations. Further details are in Ref. 9.

DEFECTS IN HgCdTe

Equilibrium native point defect concentrations: annealing studies

Gibbs' phase rule tells us that for a system of three components (in our case mercury, cadmium, and tellurium) and two phases (zincblende solid and vapor) there are three degrees of freedom. In evaluating the equilibrium defect concentrations in $Hg_{0.8}Cd_{0.2}Te$ we have chosen the temperature, the mercury pressure P_{Hg}, and the alloy composition x as these specified variables; the tellurium and cadmium pressures, the crystal stoichiometry, and the density of the various native point defects are determined by these parameters.

In Fig. 1 we show our results for the 77 K hole concentrations in $x = 0.2$ $Hg_{1-x}Cd_xTe$ as a function of mercury partial pressure for various high–temperature annealing conditions, and compare them to the results of Vydyanath.[3,13] We have assumed that the high–temperature defect structure is frozen in during a quench to 77 K. All eight point defects discussed above have been included in our analysis. The agreement with experiment is quite good, given that the only empirical data used were of the temperature dependence of the band structure used to calculate the intrinsic reaction constant. To demonstrate the sensitivity of our results to the free energies we are calculating from first principles, we have also shown in Fig. 1 the results of a calculation using a mercury vacancy formation energy that has been increased roughly 10%, plus a constant multiplicative constant of the low–temperature hole concentrations at all pressures and temperatures; as one can see, such minor modifications to our calculated parameters yield low–temperature hole concentrations that are in very good agreement with experiment. Certainly, refinements to our theory (for example, including a more accurate high–temperature band structure, more precise incorporation of alloy effects on formation free energies, anharmonic effects in the vibrational free energies, and going beyond the local density approximation) could account for discrepancies of this magnitude. In addition, the experimental data may be impacted by reequilibration during the quench from high temperature.

At all temperatures, we predicted that equilibrated material will be p–type and that the dominant defect is the doubly ionized mercury vacancy, in agreement with mobility data.[3] Our predictions differ from the analysis in Ref. 3 in several ways, though. First, although the data indicate that the material is intrinsic at all annealing temperatures, we predict that the material will be extrinsic for the higher annealing temperatures with $[h^\bullet] \sim P_{Hg}^{-1/3}$, while at the lower annealing temperatures the material will be intrinsic with $[h^\bullet] \sim P_{Hg}^{-1}$ (for details see Ref. 9). This may be due to either a vacancy formation energy that is too small in our calculation (as demonstrated by the dashed line in Fig. 1) or errors in the high–temperature band structure, which we have extrapolated from the low–temperature formulas.[14,15] Second, we find at higher temperatures and lower pressures, that the hole concentrations increase with increasing pressure, contrary to what would be expected due to mercury vacancy acceptors alone. In our theoretical predictions this is due to compensation from tellurium antisites, which we predict are donors, and which are the second most dominant native point defect in $Hg_{1-x}Cd_xTe$. Because the equilibrium antisite density varies roughly as P_{Hg}^{-2}, compared to P_{Hg}^{-1} to $P_{Hg}^{-1/3}$ for the mercury vacancy, it is most important at low mercury pressures. At the highest temperatures there does

appear to be a corresponding role–off in the experimental data at the lower pressures, which may be indicative of compensation by tellurium antisites, but it could also be an experimental artifact caused by quenching inefficiencies for the higher temperatures.

Low–temperature mercury–saturated anneals are of technological importance to reducing the as-grown p–type carrier concentrations or to convert the material to n–type in nominally undoped material. In Fig. 2 we have plotted the concentrations of mercury vacancies and tellurium antisites as a function of inverse temperature for constant pressures within the existence region; neither of these concentrations included the defects that are bound into mercury vacancy tellurium antisite pairs. The lower boundaries correspond to the defect densities for mercury–saturated anneals, the upper boundary to tellurium–saturated anneals. As one can see, at a given pressure and temperature, the mercury vacancy concentrations are always in excess of the tellurium antisite population, and in equilibrium the material should always be p–type. As discussed in the following section, we expect that full equilibration of the tellurium antisite density may not take place at lower annealing temperatures, so that the equilibrium concentrations predicted for this defect may not always be realized.

Annealing schedules are also of technological importance in forming p–n junctions in as–grown p–type material via mercury in diffusion.[16,17] The results of these experiments depend on the mechanism by which mercury diffuses and are related to the identity of the residual donor, both of which will be discussed further below.

The tellurium antisite in $Hg_{0.78}Cd_{0.22}Te$

Having predicted that the tellurium antisite will be present in substantial densities, we now address the evidence for their existence in LWIR HgCdTe. We have predicted that the tellurium antisite is a donor, although we have not yet extended our theory to predict whether it is a single or double donor, nor the precise location of the defect levels in the gap. This is perhaps the most difficult part of our calculation because of the LDA band gap errors intrinsic to our method and the dispersion arising from the use of supercells that give defect–level widths larger than the $Hg_{0.78}Cd_{0.22}Te$ band gap. To establish the presence of tellurium antisites without a prediction of the donor level(s) in the gap, we must consider the possibility that there are resonant level(s), shallow level(s), deep level(s), or some combination of these, associated with the tellurium antisite, and look for evidence supporting the presence of the antisite.

One of the outstanding questions in the properties of HgCdTe is the identification and elimination of the residual donor that controls the carrier concentration in material annealed at low temperatures under mercury–saturated conditions. Although purification of starting materials has led to a lowering of the residual donor density, a lower limit of $\sim 10^{14}$ cm^{-3} seems to have been reached. To examine the possibility that the tellurium antisite is the residual donor, we have calculated the defect densities at 500°C, roughly the LPE growth temperature from both the mercury– and tellurium–rich melts, at 185°C, the typical molecular beam epitaxy (MBE) growth temperature, and at 220°C, roughly where low–temperature mercury–rich anneals are done; results are shown in Fig. 3(a-c). It is clear that the material is expected to be p–type for both MBE– and LPE– grown material, and that although postgrowth, mercury–saturated anneals (the right side of Fig. 3(c)) will lower the vacancy density below the 10^{13} cm^{-3} level, the material is still predicted to be mercury–vacancy–doped p–type. We thus conclude that the residual donor is not due to an equilibrium concentration of native point defects.

The possibility remains that the residual donor is associated with a nonequilibrium

defect concentration of tellurium antisites. We expect that the diffusion coefficient of the tellurium antisite is relatively small because the diffusion of an antisite will necessarily involve at least one additional point defect, such as the mercury vacancy or the tellurium interstitial (diffusion via a consorted exchange of a tellurium antisite with a mercury atom on an adjacent cation lattice site is unlikely). As such, the tellurium antisite may not reach equilibrium densities for the times and temperatures corresponding to the low–temperature mercury–saturated anneals typically employed to equilibrate the mercury vacancy density (Fig. 3(c)). If tellurium antisite densities are in fact equilibrated at a temperature at which the antisite diffusion effectively stops during cooldown from the growth temperature, then the antisites may be frozen in at higher, nonequilibrium concentrations corresponding to the residual donor density.

Addressing the question as to why the antisite density might be frozen in at roughly the same concentration for LPE material grown from both the mercury and tellurium melt, we return to the means by which tellurium antisite diffuses in the material, and assume it diffuses by a mercury vacancy mechanism. This assumption is motivated by several factors. First, this mechanism involves only one point defect in addition to the tellurium antisite, and involves a simple migration mechanism between the two defects. Second, it involves the mercury vacancy, whose density is fairly high, and therefore the probability of tellurium antisite mercury vacancy pairs is expected to be fairly high. In addition, the mercury vacancy is an acceptor and the tellurium antisite is a donor so they are expected to form a bound pair based on Coulombic attraction, and the mercury vacancy is too small for the lattice, while the tellurium antisite is too large, so that there is a mechanical attraction between them as well. Finally, the migration mechanism involving an interstitial—for example, via a kickout mechanism whereby a mercury interstitial kicks out the tellurium antisite to form a tellurium interstitial—is unlikely since it involves defects that are all too large for the lattice and are donors and therefore are unlikely to form pairs. The kickout mechanism may be important when mercury interstitials are injected into the material, and is discussed later in this paper. The likelihood of the tellurium antisite diffusion proceeding by the mercury vacancy mechanism is further supported by our preliminary prediction of the mercury vacancy tellurium antisite binding energy of 1.1 eV; the corresponding densities are shown in Fig. 3. We show our predictions for the pair density as a range in which the lower limit corresponds to the defect pair being neutral, as our preliminary predictions indicate, and the upper limit corresponding to the pair having a donor state at the valence band edge and an acceptor level at the conduction band edge. Unlike the native point defects, we expect that these pair defect concentrations may change as we refine the free energy calculations. If tellurium antisite diffusion is via the mercury vacancy, the diffusion coefficient will be proportional to the density of the mercury vacancy tellurium antisite pairs, that is

$$D_{\mathrm{Te_{Hg}}} \sim [(V_{\mathrm{Hg}} + \mathrm{Te_{Hg}})_{pair}]. \tag{6}$$

From Fig. 3(a) for LPE growth, one can see that the density of defect pairs for low mercury pressures, corresponding to material grown from the tellurium–rich melt, is four orders of magnitude higher than for that grown from the mercury–rich melt. This implies that although material grown from the tellurium melt will contain higher densities of tellurium antisites, in the cooldown from the growth temperature the tellurium antisites will reequilibrate much more rapidly due to the large pair density than will material grown from the mercury–rich melt. In contrast, for material grown from the mercury melt, the tellurium antisites present at the growth temperature, although lower, may be frozen in

because the pair density is also lower.

We now turn to growth by MBE, which takes place at 185°C under mercury–poor conditions, corresponding to the left side of Fig. 3(b). At the phase stability boundary, we predict that the material will be mercury–vacancy doped p–type, with a carrier concentration of $\sim 10^{15}$ cm^{-3}. Experimentally as–grown material is found to be either n– or p–type with carrier concentrations in the 10^{15} cm^{-3} range.[18] Because MBE growth is a nonequilibrium process, it is possible that growth may take place beyond the existence region; for example, if the equivalent pressure were of the order of 10^{-7} atm at 185°C, the materials would be tellurium antisite doped. While this provides a possible explanation of how the material could be n– or p–type as grown based on equilibrium concentrations of defects, extending this argument, one would expect under some growth conditions to be able to obtain highly compensated material with very low carrier concentrations; this is never seen, to our knowledge. A more likely possibility is that nonequilibrium densities of point defects are frozen into the MBE material resulting from details of the surface kinetics.

There is substantial experimental evidence of deep levels in LWIR HgCdTe, which have not yet been definitively associated with any particular defect. The minority carrier lifetimes in vacancy–doped material are limited by Shockley–Read recombination; deep–level transient spectroscopy (DLTS) measurements[19,20,21] have identified two donor-like defect levels at $0.4E_{gap}$ and $0.75E_{gap}$. The densities of these levels roughly track the mercury vacancy concentration, although substantial scatter in the correlation is observed.[19] Neither of these levels is believed to be associated with the mercury vacancy itself, nor do they appear to be associated with the same defect because they do not track one another. In equilibrium, the tellurium antisite density will track with the mercury vacancy concentration, although it will show a sharper dependence on the mercury pressure. In addition, as discussed above, we do not expect that equilibrium concentrations of tellurium antisites will be present except at very high temperatures corresponding to liquid-phase growth, and thus the ratio of tellurium antisites to mercury vacancies expected in equilibrium may not be experimentally realized, leading to substantial deviations from the equilibrium ratio, and scattering in their concentrations. Thus, it is plausible that one of the Shockley–Read recombination centers is associated with the tellurium antisite, although to confirm this possibility a more quantitative prediction of the ionization levels of the antisite is needed. Deep levels associated with the tellurium antisite may also be responsible for the $1/f$ noise, which is found to be roughly proportional to the mercury vacancy concentration[22] or they may enhance interband tunneling and thereby contribute to dark currents.

The role of native point defects in self-diffusion

Self-diffusion of mercury is important for the annealing of as–grown mercury–vacancy doped p–type material to n–type, to form p–n junctions,[16] and for understanding junction stability in HgCdTe devices. Although both the mercury vacancies and interstitials are mobile and contribute to mercury diffusion,[23] it is the interstitial diffusion that is found to dominate in the modeling of low–temperature anneals.[12,17] Thus, although we find equilibrium mercury interstitial concentrations that are negligible in terms of their contribution to the net carrier densities,[9] they will be important to mercury transport in the material, and therefore their properties are of interest. For both mercury vacancy and interstitial diffusion, more than just defect concentrations enter into the determination of the diffusion coefficients; for the present discussion, we will address only how our defect

concentrations relate to the measured diffusion coefficients.

We predict that mercury interstitials are donors and in equilibrium are present in concentrations that are less than 10^6 cm^{-3} at 250°C.[9] We have compared our results with those of annealing simulations by the Stanford group[12] and find that the concentration of interstitials we have predicted at $\sim$ 200°C are several orders of magnitude too small to account for their modeling of the formation of p–n junctions. Although a number of approximations in our calculation of the formation energies will affect our interstitial formation free energy (for example, the use of supercells and approximations of the ionization energies) we do not expect these to account for this large a discrepancy. As discussed in the Methodology section above, we have completed the calculation of the electronic contribution to the formation free energies using pure HgTe. For the mercury vacancy and the tellurium antisite that are the major defects in HgCdTe and that occupy the cation sublattice and therefore are surrounded by four tellurium atoms, this is probably not such a bad assumption. Corrections to the electronic energy due to the presence of cadmium may be larger for the interstitials that see four cations as their first nearest neighbors in one tetrahedral site and six cations as near second neighbors in the other tetrahedral site. We are currently calculating the correction to our electronic energies, taking explicit account of cadmium in the lattice to see if it will eliminate the discrepancy with the Stanford model predictions.[12]

There has been a recent investigation[24] in $x = 0.22$ and 0.24 $Hg_{1-x}Cd_xTe$ on samples in which high concentrations of nonequilibrium mercury interstitials have been introduced. The observed deep levels near 45 and 60 meV above the valence-band edge were argued to be associated with the mercury interstitials. As discussed above, at this point our calculations are not able to determine the precise positions of the defect levels in the gap, but rather have predicted only that the mercury interstitials will be donor-like. If in fact there are donor levels associated with the mercury interstitials that are near midgap, we would expect them to exhibit a series of levels corresponding to the different alloy environments about an interstitial. In addition, there are two classes of interstitials that we expect to have relatively high equilibrium densities, both of which occupy tetrahedral sites; the first is surrounded by four cation nearest neighbors, and the second is surrounded by four anion nearest neighbors. Although it is tempting to associate the two defect levels experimentally observed with these two classes of interstitial sites, there is no apparent reason why two levels are seen in the $x = 0.22$ material and only one level in for $x = 0.24$.

Finally, we return to the discussion of the mechanism for tellurium antisite diffusion and readdress the kickout mechanism that proceeds via the reaction

$$\mathrm{Hg}_I + \mathrm{Te}_{\mathrm{Hg}} \rightarrow \mathrm{Te}_I. \tag{7}$$

Our calculations predict that this is an exothermic reaction, with an energy of ~ 0.8 eV (the entropy gained in having two point defects rather than just one must also be considered in establishing the equilibrium concentrations of these defects). In nonequilibrium situations in which mercury interstitials are introduced into the material—for example, during ion-beam milling or oxide baking[25]— this reaction will be pushed to the right, and excess tellurium interstitial will be produced. Thus, in such situations, one might expect tellurium antisite diffusion via the kickout mechanism to be a stronger competitor to the mercury vacancy mechanism, although the barriers to the formation of Hg_I–$\mathrm{Te}_{\mathrm{Hg}}$ pairs still exist, as discussed above.

In presenting the tellurium antisite as a candidate for the residual donor we argued why its density might be fixed in the n–type material. On the other hand, when discussing

the possibility that it is related to a Shockley–Read recombination center in vacancy-doped p–type material, we argued why its density might vary, depending on the cooldown rate and so forth. These two arguments are somewhat inconsistent. Although the possibility still exists that the tellurium antisite is both the residual donor (via a first ionization level that resonates in the gap) and a Shockley–Read center (via a midgap second ionization level), to be convincing a firmer correlation between the two would have to be established.

The mercury vacancy tellurium antisite pair

Several additional consequences of the presence of the mercury vacancy tellurium antisite pairs should be discussed. As one can see from Fig. 3, we are predicting a very large concentration of the defect pairs, which may even exceed the mercury vacancy concentrations for LPE material grown from the tellurium–rich melts. If the pair is electrically inactive, as our preliminary calculations predict, it will not impact the carrier concentrations or mobility. Such a large density of pairs does imply that the nonstoichiometry of the material is larger than that due to the vacancy concentrations, particularly at lower temperatures where we predict that the equilibrium concentrations of neutral pairs will approach that of the mercury vacancy.

Note that the large binding energy of the mercury vacancy tellurium antisite pair suggests that other bound pairs may be present in the material. For example, a bound Frenkel defect (involving the mercury vacancy–mercury interstitial pair) that involves an acceptor and a donor defect with opposite lattice strains may be important, and will impact diffusion of mercury in the lattice. The most likely consequences will be to increase the annihilation capture cross section of mercury interstitials into mercury vacancies and to present a barrier to the formation of free Frenkel defects through a geminate process. These phenomena will be important to understanding diffusion in HgCdTe.[12] Evidence for the mercury vacancy substitutional indium pair has been seen using a nuclear hyperfine technique.[26] This defect is similar to the mercury vacancy tellurium antisite pair, and thus we expect it may be well bound. Both of these pairs merit further investigation.

DEFECTS IN CdTe

Like HgCdTe, CdTe has a wide stability region and can be doped both p– and n–type. Its use as both a substrate (along with $Cd_{1-x}Zn_xTe$[27]) and a passivant make it an important material in the manufacturing of HgCdTe LWIR FPAs.

We have predicted the density of neutral native point defects in CdTe as a function of temperature and pressure; results for 700°C are shown in Fig. 4. We predict the same electrical type (donor versus acceptor) for the native point defects as in HgCdTe; for example we find that the cadmium vacancy is an acceptor and the cadmium interstitial and tellurium antisite are donors. Based on the neutral native point defects we expect that CdTe solid can exist with both excess cadmium and excess tellurium. We find that the cadmium interstitial is the dominant defect for high cadmium pressures, and the cadmium vacancy is most important at mid and low cadmium pressures.

Because the native point defects may have energy levels in the gap associated with them, it is important to include these in the analysis. We have begun to calculate the ionization levels associated with the native point defects, but have not yet included the Jahn-Teller distortions,[28] which can significantly alter the localized energy levels. For this discussion we shall assume that the cadmium vacancy has a first ionization level near the valence-band edge and a second level near midgap,[29] and assume that the cadmium interstitial is a double shallow donor.[2] In this case we predict a p– to n–type conversion

at 700°C at relatively high cadmium pressures, in agreement with experiment.[2]

From Fig. 4 we see that the tellurium antisite becomes more important as the cadmium pressure is lowered. Depending on the energies associated with the tellurium antisite donor levels, the material may be highly compensated at the lowest pressures, or another p– to n–type conversion may even occur. Experiments designed to equilibrate on the cadmium-poor side of the stability region can be used to test for the presence of tellurium antisites through both their impact on electrical activities and the presence of localized levels.

CONCLUSIONS AND SUGGESTED EXPERIMENTS

The theory developed here clearly indicates that in $Hg_{0.8}Cd_{0.2}Te$ equilibrated at typical annealing temperatures and pressures (the right side of Fig. 3(c)) the tellurium antisite and mercury vacancy tellurium antisite pair densities are well below levels that can impact device performance. The primary outstanding question is whether or not tellurium antisite diffusion rates are high enough that normally processed samples fully equilibrate. Experiments are needed to modify these defect populations in a controlled manner so their impact on carrier concentrations, lifetimes, and other device properties can be determined. The basic idea is to modify the tellurium antisite concentration by choosing annealing temperatures, mercury pressures, and times that are long enough to permit a measurable portion of samples to equilibrate.

First we consider annealing experiments to test for the possibility that the antisite is the residual donor. If tellurium antisite diffusion is so slow that it is not equilibrated during low–temperature mercury–saturated anneals, one must first anneal at higher temperatures and lower mercury pressures to introduce tellurium antisite mercury vacancy pairs (this step could be eliminated for LPE material grown from the tellurium melt), followed by a lower–temperature, low–mercury–pressure anneal to reduce the antisite density, while still maintaining a relatively high density of pairs, concluded by a low–temperature, mercury–saturated anneal to reduce the mercury vacancy concentration even further. A series of experiments in which the conditions of the first two anneals were varied could be designed to test for the effect they have on the residual donor concentration. A similar experiment could be performed to correlate the Shockley–Read center in mercury–vacancy–doped material with nonequilibrium tellurium antisite densities.

Although we have proposed a series of experiments to establish whether the tellurium antisite is the residual donor or a Shockley–Read recombination center based on nonequilibrium densities, one may be able to design a series of experiments in which equilibrium populations of tellurium antisites are obtained by choosing high enough temperatures, thin enough samples, and long enough annealing times. One could choose annealing conditions to manipulate the mercury vacancy and tellurium antisite populations independently. For example a 300°C anneal to reduce the hole concentration to $\sim 10^{16}$ will result in an order–of–magnitude more tellurium antisites than an anneal at 400°C to achieve the same hole concentration; Fig. 2 can be used in guiding such a study. The correlation of the tellurium antisite densities with the Shockley–Read center should be possible by doing minority carrier lifetime and/or DLTS measurements on materials with the same mercury vacancy hole concentrations achieved by anneals at different temperatures. Although a study of this type was recently presented,[1] and for a given hole concentration a correlation of lifetimes with the annealing temperature was observed, the effective annealing conditions there were set by the stoichiometry of CdTe cap layers and thus were more complicated than a simple anneal with a controlled mercury overpressure.

Experiments to test the presence of the mercury vacancy tellurium antisite pair are

similar to those proposed above for the isolated tellurium antisite. Our preliminary calculations indicate that the pair will be electrically inactive and have no states in the band gap. As such, we do not expect their presence to have a direct impact on the electrical properties, but their presence will be manifested in their impact on tellurium antisite diffusion. Note that these experiments proposed to test for the presence of the tellurium antisite cannot discriminate between the isolated tellurium antisite and the mercury vacancy tellurium antisite pair.

ACKNOWLEDGMENT

The work reported here was supported by NASA Contract No. NAS1-18226, ONR Contract No. N00014-89-K-132, and ARPA Contract No. MDA972-92-C-0053. Use of the Numerical Aerodynamic Simulation supercomputer facilities at NASA Ames Research Center is gratefully acknowledged.

REFERENCES

1 C. F. Wan, M. C. Chen, J. H. Tregilgas, T. W. Orent, and J. D. Luttmer, *1993 MCT Workshop.*

2 H. R. Vydyanath, J. Ellsworth, J. J. Kennedy, B. Dean, C. J. Johnson, G. T. Neugebauer, J. Sepich, and P.-K. Liao, *J. Vac. Sci. Technol. B* 10, 1476 (1992).

3 H. R. Vydyanath, *J. Electrochem. Soc.* 128, 2609 (1981).

4 F. A. Krõger, *The Chemistry of Imperfect Crystals* (J. Wiley & Sons, Inc., New York, 1964).

5 T. Tung, M. H. Kalisher, A. P. Stevens, P. E. Herning, *Mat. Res. Soc. Symp. Proc.* 90, 321 (1987) and references therein.

6 O. K. Andersen, O. Jepsen, and D. Glotzel, *Highlights of Condensed Matter Theory*, F. Bassani *et al.*, Amsterdam, North Holland (1985) p. 59.

7 D. Langreth and D. Mehl, *Phys. Rev. B* 28, 1809 (1983).

8 M. van Schilfgaarde, A.T. Paxton, M. A. Berding, and M. Methfessel (in preparation).

9 M. A. Berding, M. van Schilfgaarde, and A. Sher, *Phys. Rev. B* 50, 1519 (1994).

10 In Ref. 9 we assumed degeneracies of one, two, and one for the neutral, singly, and doubly ionized states of all donor and acceptors in HgCdTe. This is valid if only the a_1 states are occupied and the triply (sixfold including spin) degenerate t_2 states remain unoccupied. (Recall that the point group of an undistorted point defect is T_d.) If the t_2 states are partially occupied, an additional degeneracy will be present that should be included in our calculations; this degeneracy was not included in Ref. 9 but will be added in this paper. For an undistorted defect with the full T_d symmetry, this degeneracy arises from the partial occupation of the sixfold degenerate state (constrained to have a maximal number of spins paired); if the local symmetry is lowered due to a Jahn-Teller distortion (to point group D_{2d} for one or two electrons in the t_2 state, to point group C_{2v} for three, four or five electrons in the t_2 state[11]), this additional degeneracy arises from the extra degree of freedom present in the introduction of a locally preferred direction in space. Going through the counting, we obtain degeneracy factors of (6,3,6,3,6,1) for one to six electrons in the t_2 state, respectively. Results reported here include these full degeneracy factors.

11 See, for example, the discussion of symmetry–lowering distortions in silicon in G. A. Baraff, E. O. Kane, and M. Schlüter, *Phys. Rev. B* 21, 5662 (1980).

12 S. L. Holander and C. R. Helms, private communication.

13 H. R. Vydyanath and C. H. Hiner, *J. Appl. Phys.* 65, 3080 (1989).

14 G. L. Hansen and J. L. Schmit, *J. Appl. Phys* 54, 1639 (1983).

15 G. L. Hansen, J. L. Schmit, and T. N. Casselman, *J. Appl. Phys.* 53, 7099 (1982).
16 H. F. Schaake, J. H. Tregilgas, J. D. Beck, M. A. Kinch, and B. E. Gnade, *J. Vac. Sci. Technol. A* 3, 143 (1985); H. F. Schaake, *J. Electron. Mater.* 14, 513 (1985).
17 J. L. Meléndez and C. R. Helms, *J. Electron. Mat.* 22, 999, (1993).
18 See, for example, R. Sporken, M. D. Lange, S. Sivanathan, and J. P. Faurie, *Appl. Phys. Lett.* 59, 81 (1991).
19 C. E. Jones, V. Nair, and D. L. Polla, *Appl. Phys. Lett.* 39, 248 (1981).
20 C. E. Jones, V. Nair, J. Lindquist, and D. L. Polla, *J. Vac. Sci. Technol.* 21, 187 (1982).
21 C. E. Jones, K. James, J. Merz, R. Braunstein, M. Burd, M. Eetemadi, S. Hutton, and J. Drumheller, *J. Vac. Sci. Technol. A* 3, 131 (1985).
22 R. Schiebel and D. Bartholomew, this conference.
23 See, for example, D. A. Stevenson and M.-F. S. Tang, *J. Vac. Sci. Technol. B* 9, 1615 (1991).
24 C. L. Littler, E. Maldonado, X. N. Song, Z. Yu, J. L. Elkind, D. G. Seiler, and J. R. Lowney, *J. Vac. Sci. Technol. B* 10, 1466 (1992).
25 J. L. Elkind, *J. Vac. Sci. Technol. B* 10, 1460 (1992).
26 W. C. Hughes, M. L. Swanson, and J. C. Austin, *Appl. Phys. Lett.* 59, 938 (1991); J. Electron. Mat. 22, 1011 (1993).
27 Because of the low zinc concentrations, our results should be applicable to $x = 0.04$ $Cd_{1-x}Zn_xTe$, which is the more recent substrate of choice for LWIR $Hg_{0.8}Cd_{0.2}Te$ devices.
28 The Jahn-Teller distortion most certainly exists at low temperatures. At high temperatures corresponding to liquid phase growth, these disortions may get washed out by thermal vibrations in the lattice. We are currently examining this issue.
29 P. Höschl, R. Grill, J. Franc, P. Moravec, and E. Belas, *Mat. Sci. and Engr.* B16, 215 (1993).

FIGURE CAPTIONS

Fig. 1. Hole concentrations at 77 K as a function of mercury partial pressure for material annealed at high temperatures, as indicated. Experimental data were taken from Vydyanath.[3] Results of our theory are shown as solid lines. To demonstrate the sensitivity of our predictions to small changes in the calculated formation free energies, we show the dashed lines, which are the theoretical results, but with the mercury vacancy formation energy increased by 10% and including a rigid upward shift of the hole concentrations by a factor of 5.5. Note that the results shown here differ from those in Ref. 9 because the inclusion of the additional degeneracy factor for the singly ionized tellurium antisite.[10]

Fig. 2. Total mercury vacancy (solid line) and tellurium antisite (dashed line) densities as a function of mercury partial pressures (atm). Full equilibration of all defects is assumed at all temperatures (see text for further discussion).

Fig. 3. The concentration of native points as a function of mercury pressure within the phase stability region at (a) 500°C, corresponding to the LPE growth temperature, (b) 185°C, the growth temperature for MBE, and (c) 220°C, a typical temperature for mercury–saturated anneals. A range of concentrations for the mercury vacancy tellurium antisite pair is shown, based on our preliminary results, as discussed in the text.

Fig. 4. Neutral native point defect densities of CdTe within the stability region at 700°C.

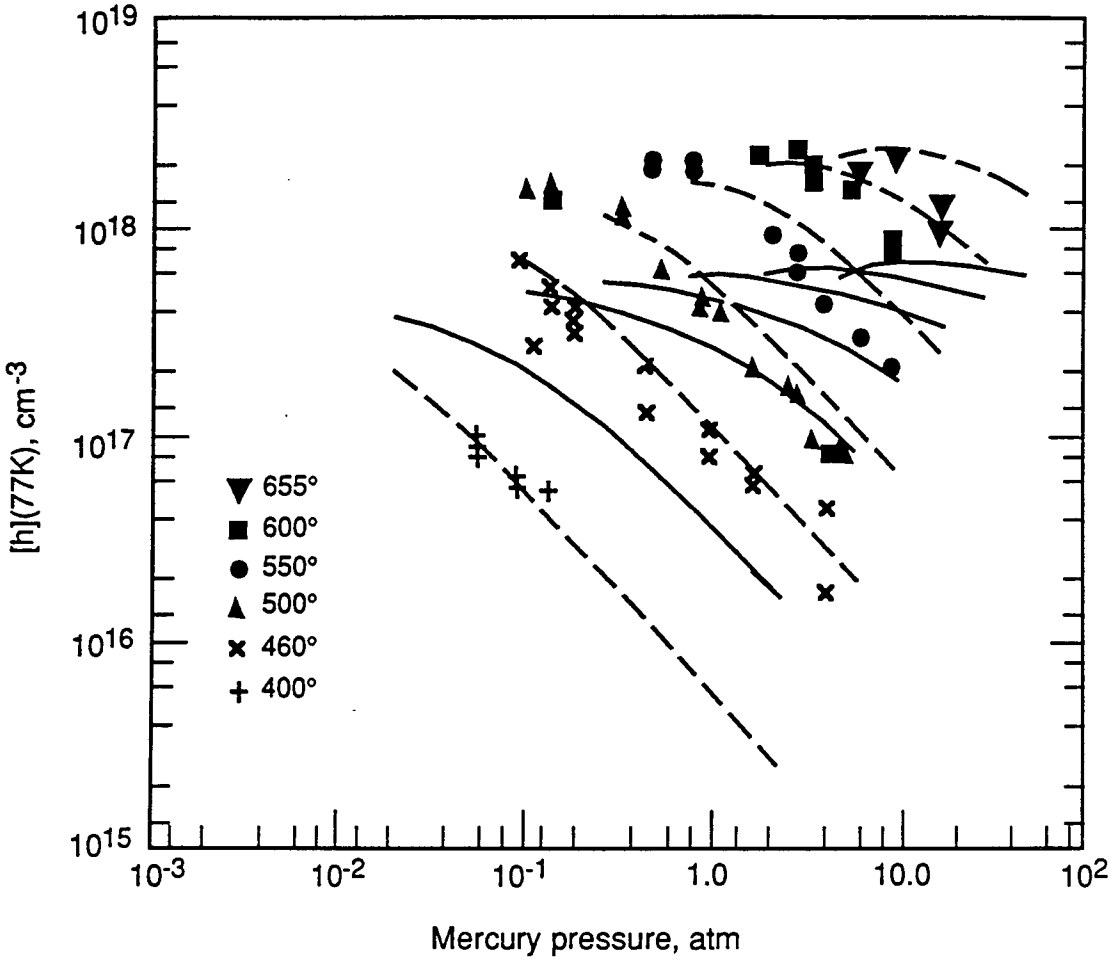
10^{19}
10^{18}
10^{17}
10^{16}
10^{15}
[h](77K), cm^{-3}
655°
600°
550°
500°
460°
400°
10^{-3}
10^{-2}
10^{-1}
1.0
10.0
10^{2}
Mercury pressure, atm

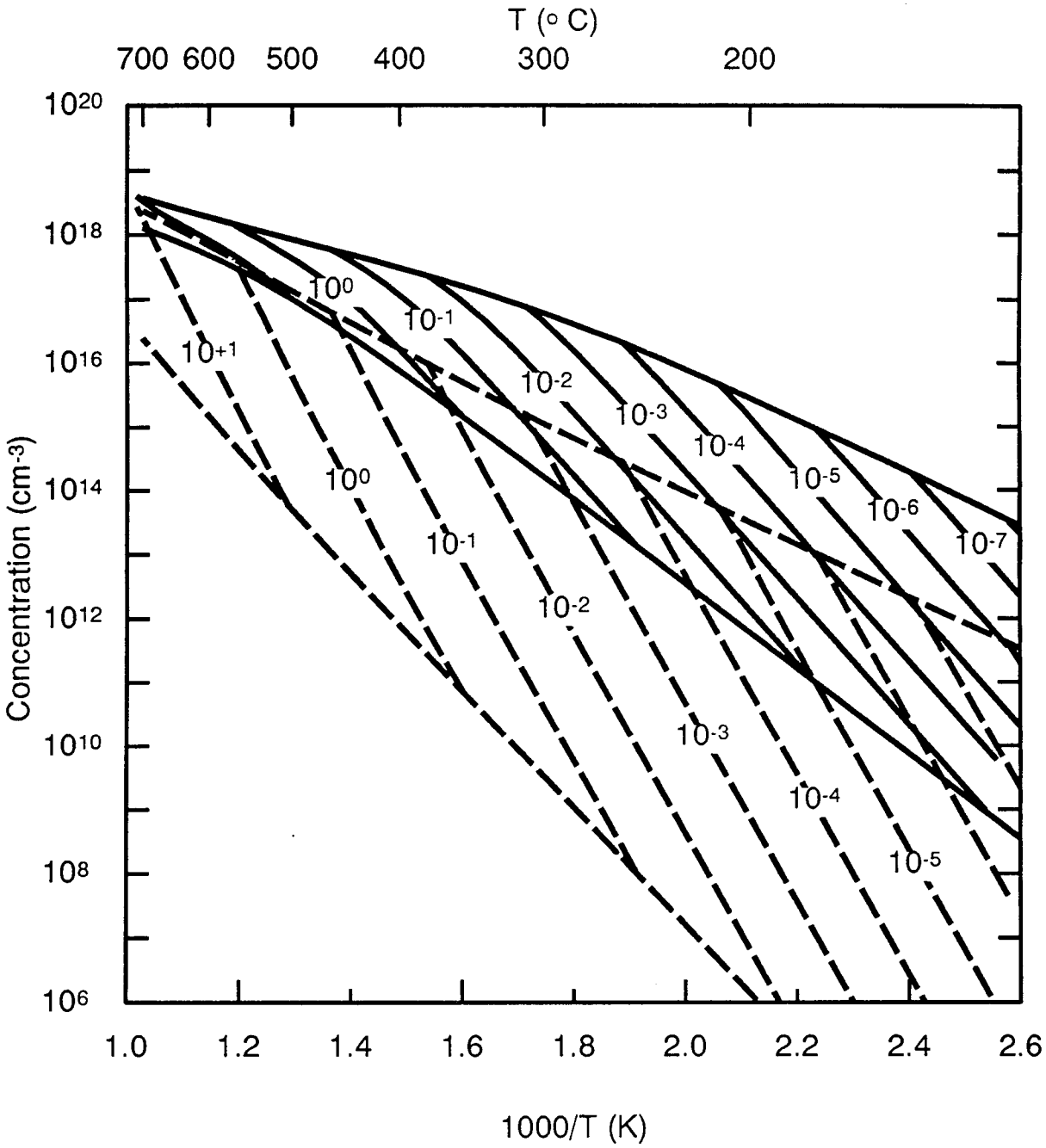
T (° C)
700 600 500 400 300 200
10^{20}
10^{18}
10^{16}
10^{14}
10^{12}
10^{10}
10^{8}
10^{6}
Concentration (cm^{-3})
10^{+1}
10^{0}
10^{-1}
10^{-2}
10^{-3}
10^{-4}
10^{-5}
10^{-6}
10^{-7}
1.0 1.2 1.4 1.6 1.8 2.0 2.2 2.4 2.6
1000/T (K)

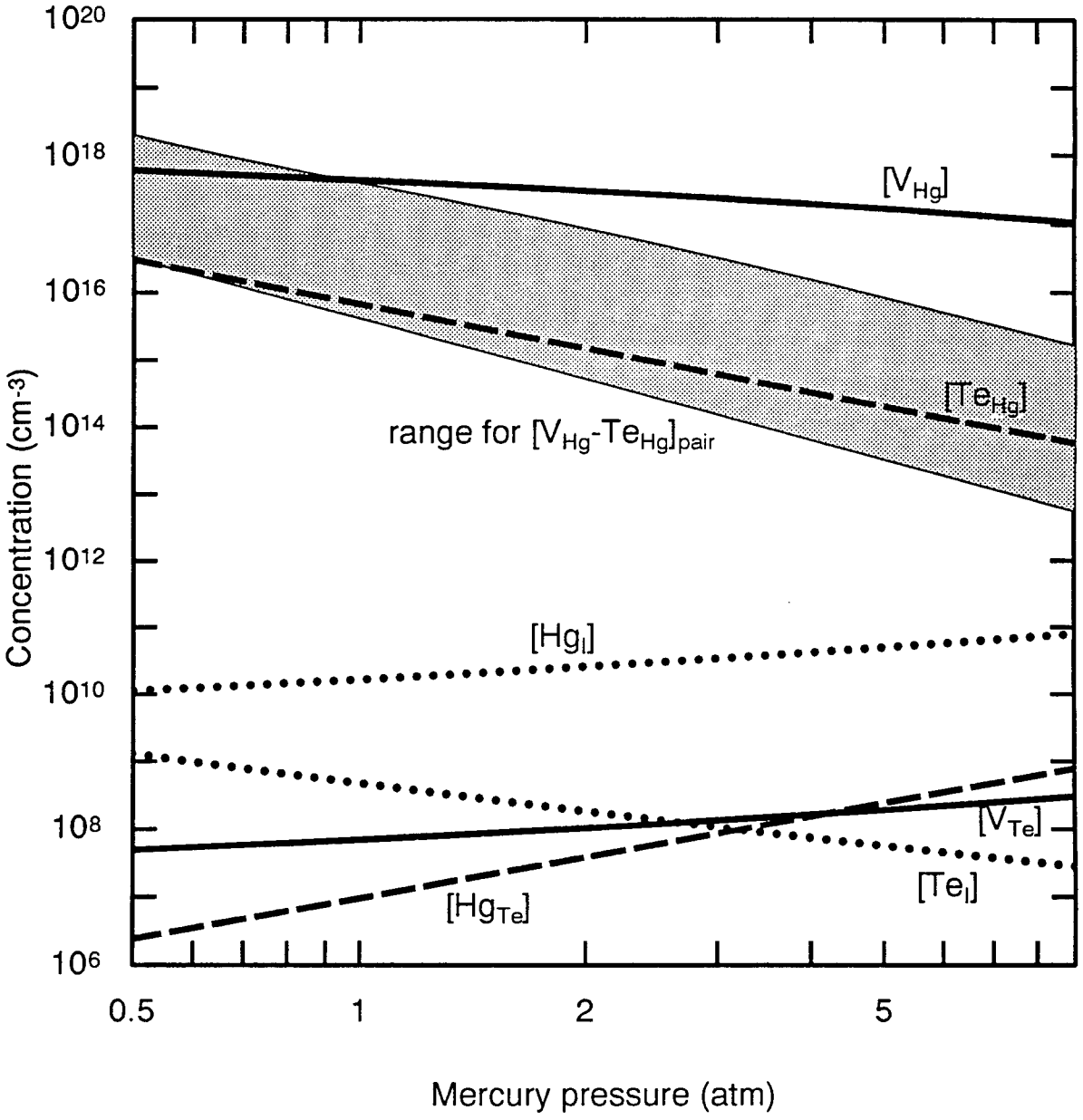
10^{20}
10^{18}
10^{16}
10^{14}
10^{12}
10^{10}
10^{8}
10^{6}
Concentration (cm^{-3})
$[V_{Hg}]$
$[Te_{Hg}]$
range for $[V_{Hg}\text{-}Te_{Hg}]_{pair}$
$[Hg_I]$
$[V_{Te}]$
$[Te_I]$
$[Hg_{Te}]$
0.5
1
2
5
Mercury pressure (atm)

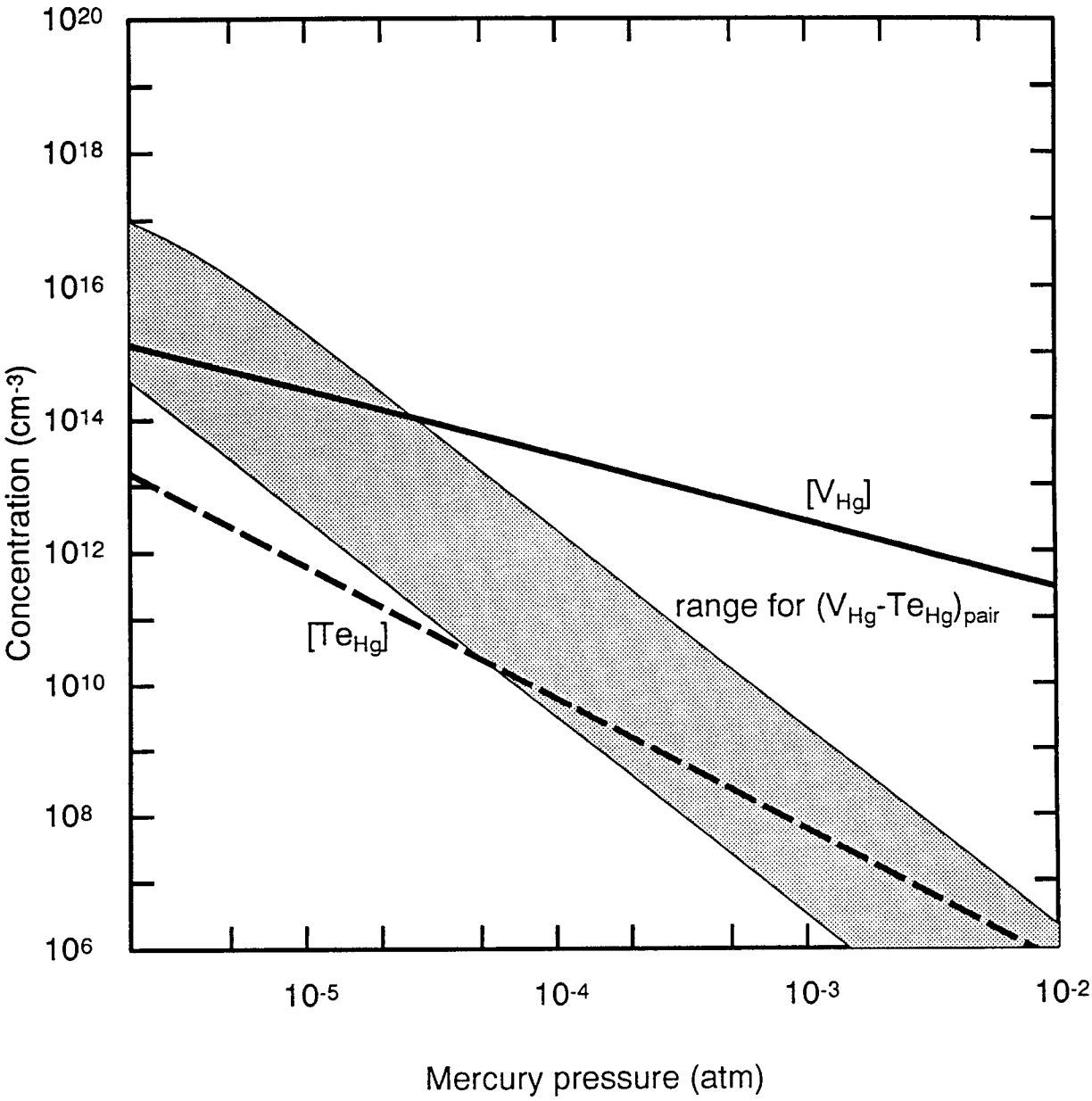
10^{20}
10^{18}
10^{16}
10^{14}
10^{12}
10^{10}
10^{8}
10^{6}
Concentration (cm^{-3})
$[V_{Hg}]$
range for $(V_{Hg}\text{-}Te_{Hg})_{pair}$
$[Te_{Hg}]$
10^{-5}
10^{-4}
10^{-3}
10^{-2}
Mercury pressure (atm)

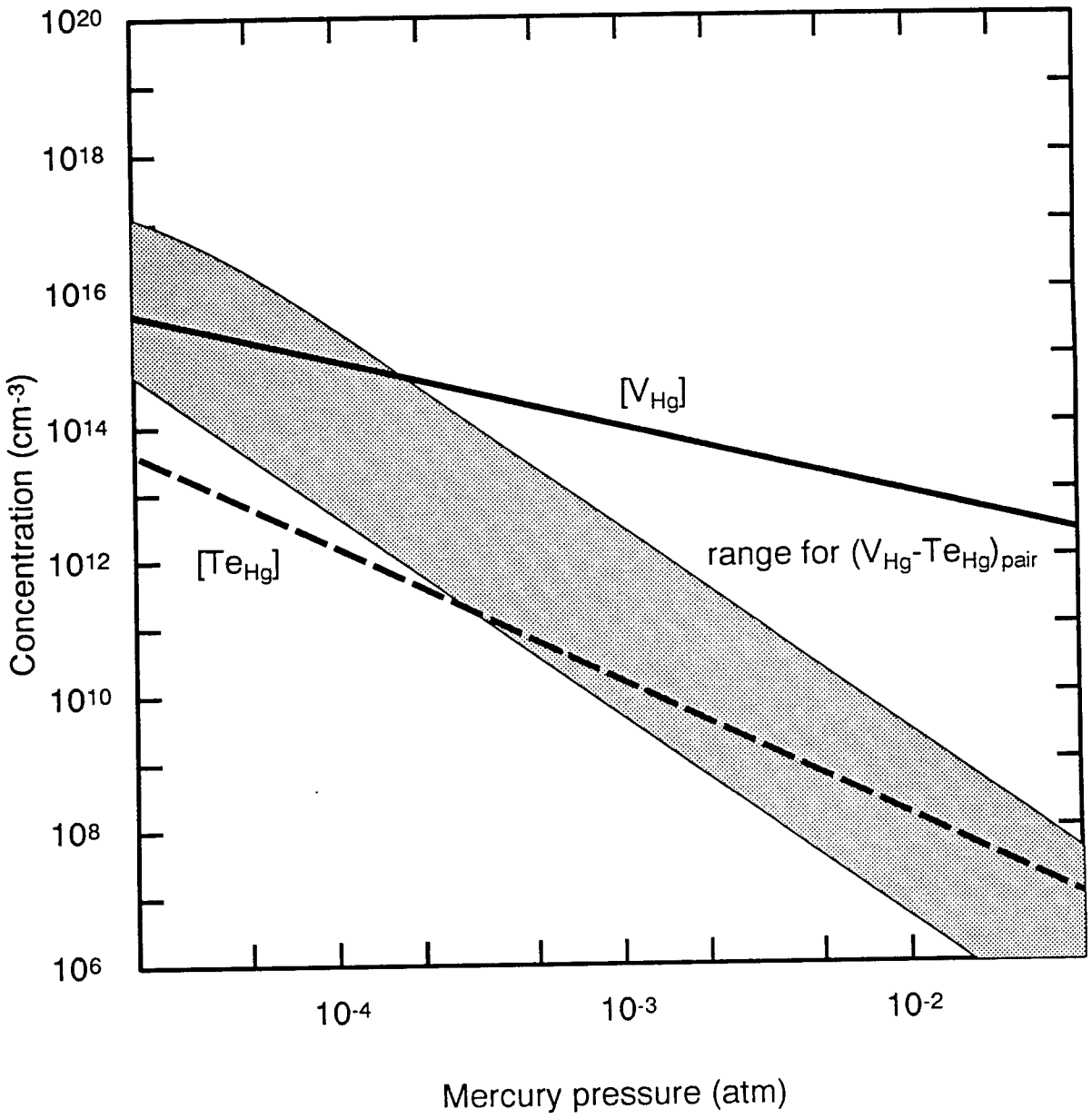
10^{20}
10^{18}
10^{16}
10^{14}
10^{12}
10^{10}
10^{8}
10^{6}
Concentration (cm^{-3})
$[V_{Hg}]$
$[Te_{Hg}]$
range for $(V_{Hg}\text{-}Te_{Hg})_{pair}$
10^{-4}
10^{-3}
10^{-2}
Mercury pressure (atm)

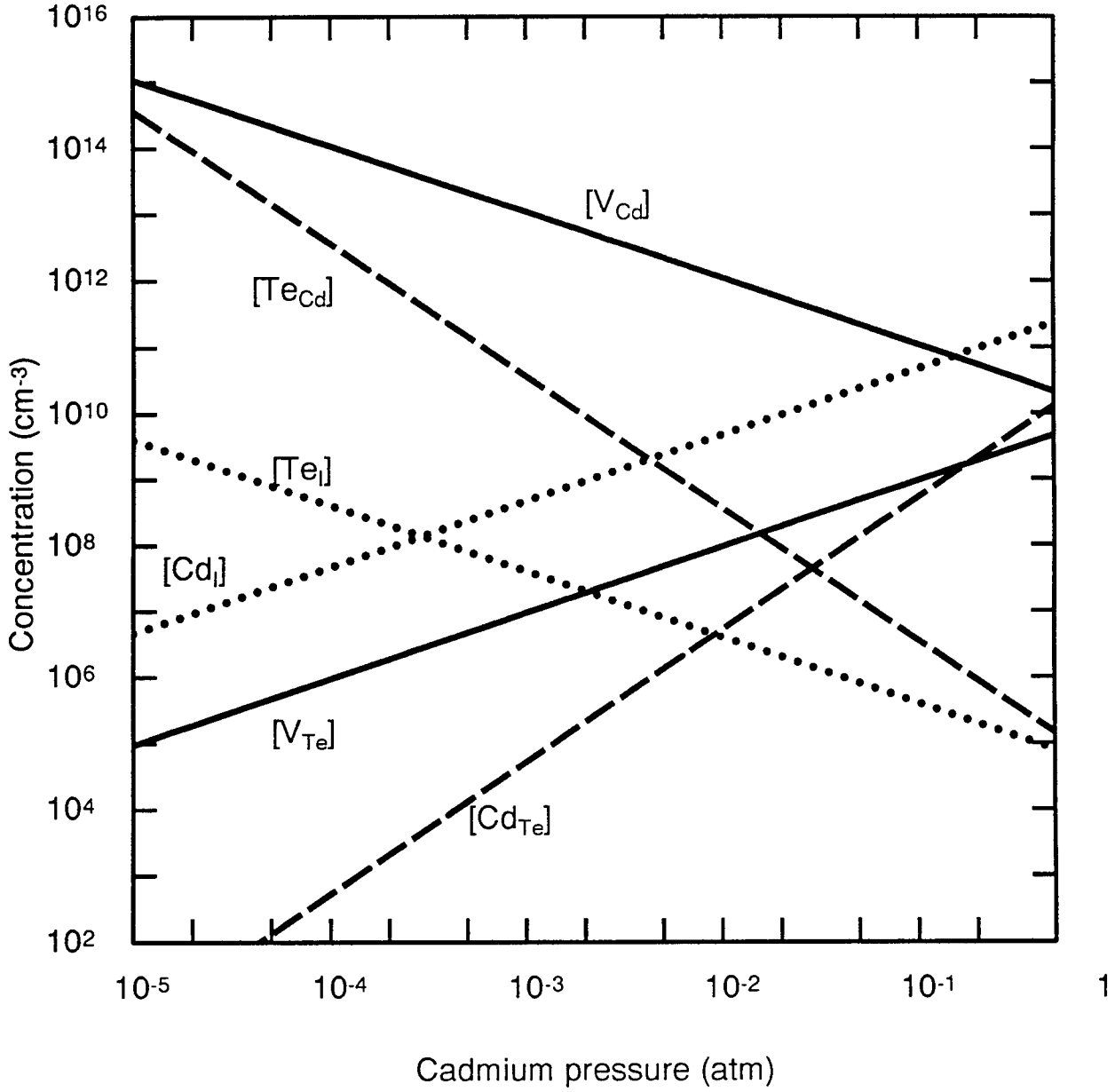
10^{16}
10^{14}
10^{12}
10^{10}
10^{8}
10^{6}
10^{4}
10^{2}
Concentration (cm^{-3})
$[V_{Cd}]$
$[Te_{Cd}]$
$[Te_I]$
$[Cd_I]$
$[V_{Te}]$
$[Cd_{Te}]$
10^{-5}
10^{-4}
10^{-3}
10^{-2}
10^{-1}
1
Cadmium pressure (atm)

APPENDIX C

Temperature dependence of the band gaps in HgCdTe and other semiconductors

Temperature Dependence of Band Gaps in Hgcdte and Other Semiconductors

Srinivasan Krishnamurthy[a], A.-B. Chen[b], A. Sher[a], and M. van Schilfgaarde[a]

[a] *SRI International, Menlo Park, CA 94025*

[b] *Physics Department, Auburn University, Auburn, AL 36349*

(September 27, 1994)

Abstract

Band-edge shifts induced by the electron-phonon interaction are calculated for HgCdTe alloys and various semiconductor compounds starting from accurate zero-temperature band structures. The calculated temperature variation of gaps agrees with experiments to better than 10% in all materials except InAs and InSb where the deviation is about 50%. While the simple picture that the intra (inter)-band transitions reduce (increase) the gap still holds, we show that both the conduction band edge E_c and valence band edge E_v move down in energy. These shifts in E_v affect the valence band offsets in heterojunctions at finite temperature. The temperature variations of valence band offset and the electron effective mass are also reported.

Key words: Temperature-dependent band structures, electron-phonon interactions, band offset, HgCdTe and alloys, III-V semiconductors

INTRODUCTION

The temperature (T) dependence of energy gaps of semiconductors is of great physical and technological interest. The quantities such as band offset and effective mass depend sensitively on the temperature variation of band edges. Numerous theoretical [1-9] and experimental [10-19] studies have been undertaken to obtain both qualitative and quantitative variations of various gaps in semiconductors. The gap decreases with increasing temperature in medium-gap and wide-gap semiconductors, and it increases in small-gap materials such as HgCdTe, PbS, PbSe, and PbTe. The thermal expansion of the lattice and electron-phonon interactions are usually considered causes for the temperature variation of the band structures. Thermal expansion always reduces gaps.

In a perturbation-theory treatment of electron-phonon interactions, the intraband transitions reduce the gap whereas interband transitions increase it, and the net shift in the gap can be positive or negative. Here we calculate the gap variation in $Hg_{1-x}Cd_xTe$ alloys, GaAs, InAs, InSb, InP, and CdTe compounds, starting from accurate band structures, wave functions, proper phonon dispersion relations, and taking account of matrix elements of the electron-phonon interactions. The contributions from each phonon branch to each electron band have been obtained to assist physical understanding of the underlying causes of the variations. We show that *both* conduction and valence band edges move down in energy. When the valence band edge moves more than the conduction band edge, the gap increases with T, as in the case of some $Hg_{1-x}Cd_xTe$ alloys with $x < 0.5$. The reverse occurs for all III-V compounds studied and $Hg_{1-x}Cd_xTe$ with $x > 0.5$. This observation has an important effect on our understanding of the variation of band offsets in semiconductor heterojunctions. In addition to the gap, other features of the band structure change with temperature and will affect the spectral variations of the absorption coefficient and transport properties.

METHOD

Our calculation of the temperature dependence of the band gap starts with accurate band structures. Empirical pseudopotential form factors are used to construct a hybrid pseudopotential tight-binding (HPTB) Hamiltonian. The pseudopotential part of the Hamiltonian is universal– it applies to all group IV, III-V and II-VI compounds. The smaller tight-binding part is expressed in a minimum set of sp^3 Slater orbitals per atom. This Hamiltonian is then transformed into an orthonormal basis. A site-diagonal spin-orbit Hamiltonian is then added. Parameters in the tight-binding perturbation are chosen to fine-tune the band structures to agree well with experiments [20,21]. Various results obtained using these band structures are found to be quite reliable [21-23]. The present study subjects the accuracy of the wave functions as well as the energies to a sensitive test.

The dilation contribution to the band gap reduction is given [5,9] by $3\alpha_T \mathrm{B}\partial E_g/\partial \mathrm{P}$, where the thermal expansion coefficient of the lattice α_T, the bulk modulus B, and the change in the gap with pressure are obtained from the literature [19]. The electron-phonon interactions with all phonon branches that cause the band structure changes are treated in perturbation theory. The total Hamiltonian is assumed to be a sum of potentials from single atoms. The atomic potential in the solid is traditionally expanded in a Taylor series, with only the leading term retained, and the energy shifts it causes are evaluated in second-order perturbation theory. However, it has been demonstrated by a number of researchers [3,4,6] that retention of first-order perturbation terms with a second term in the Taylor series expansion is necessary to preserve symmetry. We retain both terms. The change in the energy at a given wave vector k is

$$\Delta E_{n\mathbf{k}} = < n\mathbf{k}|V_2|n\mathbf{k} > + \sum_{n'\mathbf{k}'} \frac{| < n'\mathbf{k}'|V_1|n\mathbf{k} > |^2}{E_{n\mathbf{k}} - E_{n'\mathbf{k}'}} \qquad (1)$$

where V_1 and V_2 are the first two terms in the Taylor expansion of the total electron-phonon potential in powers of atomic displacements ξ. In the TB formalism, Eq. (1) can be written in terms of the matrix elements

$$< l'j'\alpha'|V_1|ljc\alpha >= \nabla V_{\alpha\alpha'}(\mathbf{d}_{ll'}^{jj'}) \cdot (\xi_{l'j'} - \xi_{lj}), \tag{2}$$

and

$$\begin{aligned} < l'j'\alpha'|V_2|ljc\alpha > \; &= \tfrac{1}{2}[\xi_{l'j'} \cdot (\nabla)^2 V_{\alpha\alpha'}(\mathbf{d}_{ll'}^{jj'}) \cdot \xi_{l'j'} \\ &\quad + \xi_{lj} \cdot (\nabla)^2 V_{\alpha\alpha'}(\mathbf{d}_{ll'}^{jj'}) \cdot \xi_{lj}], \end{aligned} \tag{3}$$

where $\mathbf{d}_{ll'}^{jj'}$ is the position vector connecting atomic sites l, species (anion or cation) j and site l', species j', and $V_{\alpha\alpha'}$ $(\mathbf{d}_{ll'}^{jj'})$ is a HPTB matrix element between the orbitals α and α' located on those atoms. From the quantum theory of harmonic crystals, the atomic displacements ξ can be expressed in terms of normal modes– that is, phonons. We have

$$\begin{aligned} \xi_{lj} = [\tfrac{\hbar}{2NM_j}]^{\frac{1}{2}} \textstyle\sum_{q\lambda} \omega_{\lambda q}^{-\frac{1}{2}} [\mathbf{e}_{\lambda q}^{j} a_{\lambda q} e^{iq\cdot(l+\tau_j)} \\ + \mathbf{e}_{\lambda q}^{*j} a_{\lambda q}^{\dagger} e^{-iq\cdot(l+\tau_j)}] \end{aligned} \tag{4}$$

where $\mathbf{q}$ and ω are phonon wave vector and frequency, λ denotes phonon branch, $a(a^{\dagger})$ is a phonon annihilation (creation) operator, M is the atomic mass, and $\mathbf{e}$ is an eigenvector in a diamond or zincblende structure of the six-dimensional dynamical matrix eigenvalue problem

$$M\omega^2 \mathbf{e} = \mathbf{D}(q)\mathbf{e} \tag{5}$$

Evaluation of the matrix elements given by Eqs. (2) and (3) requires knowledge of spatial variations of the interatomic TB matrix elements $V_{\alpha\alpha'}$. In Harrison's universal TB approach [24], these matrix elements scale as d^{-2}. In our generalization, we assume that $V_{\alpha\alpha'}$ varies as d^{-m} and the repulsive first-neighbor pair energy, following Harrison's overlap argument, as η/d^{2m}. The two unknowns m and η are determined by requiring that the calculated equilibrium bond length and bulk modulus agree well with experiments. This approach, with electrons and phonons treated from the same underlying Hamiltonian, has previously been used successfully to explain hot electron transistor characteristics [23] and is also in fairly good agreement with first-principles calculations [25]. The dynamical matrix $\mathbf{D}$ is calculated from the valence force field model [26].

The calculational procedure is as follows. For a chosen material, m and η are evaluated. Then the first and second derivatives of all interatomic matrix elements are obtained. The dynamical matrix is diagonalized to obtain ω and $\mathbf{e}$ as a function of $\mathbf{q}$ and λ. The phonon structures and electronic band structures are used [Eqs. (1) through (4)] to obtain the change in the band energy at a given $\mathbf{k}$. The polar coupling terms are included in the longitudinal optical phonon contributions. When we are interested in studying the change in the direct gap, $\mathbf{k}$ is taken to be zero. However, when the temperature variation of the effective masses or indirect gap are studied, non-zero $\mathbf{k}$ values must be used and the Brillouin zone summation in Eq. (1) should be carried over the entire zone with reduced, or no, symmetry.

RESULTS

The calculated band-gap change as a function of T in $Hg_{0.78}Cd_{0.22}Te$ is shown in Fig. 1. With increasing T, the direct gap increases in $Hg_{0.78}Cd_{0.22}Te$. Notice that the calculated values are typically within 10 to 15 meV of experimental values [16-18]. The cross ($\times$) at T=0 represents the calculated zero-point correction to the gap (13.6 meV for $Hg_{0.78}Cd_{0.22}Te$). The zero-temperature band gap calculated without electron-phonon interactions should have this correction subtracted for comparison to experimental values.

The change in the gap is traditionally explained in terms of inter- and intraband interactions. The intravalence (conduction) band interactions push the valence (conduction) band edge up (down), thus reducing the gap. Similarly, the valence-conduction band interactions increase the gap. Hence, one might expect the gap to decrease in wide-gap semiconductors and possibly increase in small-gap semiconductors. In addition, arguments based only on total density of states and ignoring variations in matrix elements will predict the valence band edge E_v move up in energy, because the hole effective mass is one to two orders of magnitude larger than the electron mass. As seen from Fig. 2, our detailed calculations of band edge movements in $Hg_{0.78}Cd_{0.22}Te$ do not support this traditional view. We find that

at high temperatures (>150 K). The calculated dE_g/dT values (circle) are compared with experiments (cross) values in Fig. 3. We see that the calculations produced correct trends in all these materials, but compare less favorably with experiments in InAs and InSb. However, it is important to note that the sign of the change is not exclusively determined by the magnitude of the zero-temperature gap. For example, although $Hg_{0.70}Cd_{0.30}Te$ and InSb have the same zero-temperature gap of 0.235 eV, the InSb gap decreases with T, whereas the $Hg_{0.70}Cd_{0.30}Te$ gap increases with T. The combination of gap size, conduction band width, and intervalley separations gives rise to these interesting variations in the gap with T.

The observation that both E_v and E_c move down in energy has an important effect on band offsets in heterojunction-based devices. For example, the zero-temperature valence band offset between $Hg_{0.78}Cd_{0.22}Te$ and CdTe is believed to be around 350 meV. However, we find that at 300 K, E_v in $Hg_{0.78}Cd_{0.22}Te$ and in CdTe moves down by 215 meV and 30 meV, respectively. If the dipole contribution remains the same, the valence band offset decreases to 165 meV at 300 K. The contention that the dipole contribution is nearly temperature independent stems from the observation that any shift in the average effective crystal potentialshould effectively be screened out, since these semiconductors are good dielectrics ($\epsilon \geq 10$). The temperature variation of the bands should be taken with respect to a fixed average potential. For our Hamiltonian, the valence band edge movements in each side of the junction are calculated with reference to a fixed average state. Thus, the calculated temperature dependence of the difference in the VB edge of the constituent heterojunction materials effectively governs the temperature dependence of the band offset. In addition to the electron-phonon interactions discussed above, lattice dilation changes the band edges differently [9]. This effect is not included here. In any case, this band offset change has important implications for the design of abrupt heterojunction IR absorption and confined well laser devices.

In principle, the band structure at any wave vector k will change with temperature. With the change in the fundamental gap, the band curvature (or effective mass) also changes thus

affecting the optical and transport properties of the material. The self-energy calculated in this method will include the effect of scattering due to phonons *and* the change in the temperature-dependent band structure self-consistently. In the case a of narrow-gap material such as $Hg_{0.78}Cd_{0.22}Te$, the effective mass alone does not explain the low-energy portion of the conduction band structure. The lowest CB energy at any k is best described by a hyperbola [27], $(\gamma \mathbf{k}^2 + c^2)^{1/2} - c$. The calculated band gap, effective mass, γ, and c as functions of T are given in Table 2. The effective mass and c are directly proportional to the gap and hence monotonically increase with T. This is expected from the $\mathbf{k} \cdot \mathbf{P}$ theory argument, but the magnitudes predicted by two theories differ. γ decreases slightly at lower temperatures and then starts to increase with T. In a previous publication [27], we had simulated these temperature variations of γ and c by adjusting the Hg concentration in HgCdTe alloys to produce proper gap at each temperature. Those values are in remarkable agreement with the values reported in Table 2. We conclude that γ and c (given in Table 2) can be interpolated to considerable accuracy for any positive gap in the HgCdTe alloys

CONCLUSIONS

Although the calculations produced correct trends in all materials, the calculated changes in the band gap of InAs and InSb were about a factor of 2 smaller than in the experiments. We find that our calculated TA phonon frequencies away from zone center in these compounds were considerably larger than those found in experiments. As noted from Table 1, a substantial contribution comes from acoustic phonons. Consequently, our theoretical values of $E_g(T)$ are smaller than in experiments. Better predictability should result from improvement in the dynamical matrix calculated from the underlying Hamiltonian. In addition, at higher temperatures higher-order perturbation terms must be included along with finite-temperature 'renormalized' bands rather than the zero-temperature bands. Such renormalization affects the monotonic change in the gap and introduces nonlinear terms.

In summary, we have calculated the temperature variations of band gaps in various semi-

conductors. A fairly accurate HPTB Hamiltonian is used in the calculation of electron and phonon structures. The calculations explain the increase in the band gap of $Hg_{0.78}Cd_{0.22}Te$, and the decrease in the band gap of all III-V compounds studied. We show that acoustic phonons make the major contribution. Contrary to traditional thinking based on total density of states arguments, we find that both the valence and the conduction band edges move down in energy. One important consequence of this observation will be in the band offsets in semiconductor heterojunction devices. Finally, there is a small and usually negligible zero-point motion contribution to low-temperature band gaps arising from electron-phonon interactions.

We thank Dr. M. Cardona of the Max Planck Institute, Stuttgart, for pointing us to several references. Funding from ONR (contract N00014-93-C-0091) and ARPA (contract MDA972-92-C-0053) is gratefully acknowledged.

REFERENCES

[1] Y. P. Varshini, Physica **34**, 149 (1967).

[2] V. Heine and J .A. Van Vechten, Phys. Rev. B**13**, 1622 (1976).

[3] P. B. Allen and V. Heine, J. Phys. C **9**, 2305 (1976).

[4] P. B. Allen and M. Cardona, Phys. Rev. B **27**, 4760 (1983).

[5] S. Gopalan, P. Lautenschlager, and M. Cardona, Phys. Rev. B **35**, 5577 (1987).

[6] M. Cardona and S. Gopalan, in *Progress on electron properties of solids*, R. Girlanda *et al.*, eds. (Kluwer Academic publishers, 1989), p. 52.

[7] R. D. King-Smith, R. J. Needs, V. Heine, and M. J. Hodgson, Europhys. Lett. **10**, 569 (1989).

[8] S. Zollner, S. Gopalan, and M. Cardona, Sol. State Comm. **77**, 485 (1991).

[9] K. J. Malloy and J. A. Van Vechten, J. Vac. Sci. Technol. B **9**, 2112 (1991).

[10] P. Lautenschlager, M. Garriga, S. Logothetidis, and M. Cardona, Phys. Rev. B **35**, 9174 (1987), and references cited therein.

[11] Z. Hang, D. Yan, F. H. Pollak, G. D. Pettit, and M. Woodall, Phys. Rev. B **44**, 10546 (1991).

[12] L. Pavisi, F. Piazza, A. Rudra, J. F. Carlin, and M. Ilegems, Phys. Rev. B **44**, 9052 (1991).

[13] E. Grilli, M. Guzzi, R. Zamboni, and L. Pavesi, Phys. Rev. B **45**, 1638 (1992).

[14] P. Y. Liu and J. C. Maan, Phys. Rev. B **47**, 16274 (1993).

[15] M. E. Allali, C. B. Sorenson, E. Veje, and P. T. Petersson, Phys. Rev. B **48**, 4398 (1993).

[16] G. L. Hansen, J. L. Schmit, and T. N. Casselman, J. Appl. Phys. **53**, 7099 (1982).

[17] D. G. Seiler, J. R.Lowney, C. L. Littler, and M. R. Loloee, J. Vac. Sci. Technol. **A 8**, 1237 (1990).

[18] J. C. Brice, *Properties of mercury cadmium telluride*, J. Brice and P. Capper, eds. (EMIS datareviews series 3, INSPEC publication, 1987), p. 105.

[19] *Landolt-Bórnstein Numerical data and functional relationships in science and technology*, Madelung, Schultz and Weiss (eds.), New series, Vol. 17 (1982).

[20] A. -B. Chen and A. Sher, Phys. Rev. B **23**, 5360 (1981).

[21] S. Krishnamurthy, A. -B. Chen, and A. Sher, J. Appl. Phys. **63**, 4540 (1988).

[22] S. Krishnamurthy, A. Sher, and A. -B. Chen, Phys. Rev. Lett., **64**, 2531 (1990); Appl. Phys. Lett **55**, 1002 (1989); Appl. Phys. Lett **52**, 468 (1988).

[23] S. Krishnamurthy, A. Sher, and A. -B. Chen, Appl. Phys. Lett. **53**, 1853 (1988).

[24] W. Harrison, *Electronic structure and properties of solids* (Freeman, San Francisco, 1980).

[25] S. Krishnamurthy and M. Cardona, J. Appl. Phys. **74**, 2117 (1993).

[26] R. M. Martin, Phys. Rev. **B1**, 4005 (1970).

[27] S. Krishnamurthy, and A. Sher, J. Elec. Materials. (in Press) Presented at the 1993 MCT workshop, Seattle.

TABLES

TABLE 1. Calculated change in the valence (v) and conduction (c) band edge energies (in meV) of $Hg_{0.78}Cd_{0.22}Te$ alloy. Contributions from interaction with various phonon modes are shown in rows 3 to 10.

band		1	2	3	4	5	6	7	8
	v	5.90	13.99	56.85	88.51	-80.26	-92.49	-97.45	-102.07
Total									
	c	1.04	2.84	17.27	34.07	-23.81	-25.43	-43.96	-42.48
	v	4.03	6.21	30.06	41.52	-49.86	-62.17	-61.04	-49.62
TA									
	c	0.26	0.65	12.41	27.47	-3.58	-14.81	-24.50	-15.40
	v	0.91	3.18	3.14	10.53	-10.63	-5.92	-11.41	-20.59
LA									
	c	0.56	1.29	1.27	1.72	-14.94	-3.00	-2.66	-7.17
	v	0.33	2.11	6.12	11.22	-9.52	-4.98	-11.80	-17.40
LO									
	c	0.13	0.63	0.75	0.44	-3.78	-2.45	-1.18	-7.31
	v	0.63	2.48	17.53	25.24	-10.26	-19.42	-13.20	-14.45
TO									
	c	0.10	0.27	2.84	4.44	-1.52	-5.16	-15.62	-12.59

TABLE 2. Calculated E_g [meV], γ [eV^2], c[eV] and the effective mass ratio of $Hg_{0.78}Cd_{0.22}Te$ alloy as functions of temperature. $m^*(0)$ is 0.008. The zero point correction is 13.6 meV.

T	E_g	γ	c	$m^*(T)/m^*(0)$
1.00	113.60	47.7656	0.0588	1.0000
10.00	112.67	47.7553	0.0588	1.0005
20.00	112.56	47.7169	0.0592	1.0072
30.00	114.44	47.6421	0.0598	1.0199
40.00	117.15	47.5582	0.0607	1.0361
50.00	120.42	47.4461	0.0615	1.0532
60.00	123.96	47.3310	0.0624	1.0714
70.00	127.65	47.2091	0.0634	1.0904
80.00	131.44	47.0821	0.0643	1.1095
90.00	135.28	46.9418	0.0653	1.1288
100.00	139.17	46.7964	0.0662	1.1483
150.00	158.85	46.1544	0.0712	1.2529
200.00	178.73	45.5930	0.0767	1.3669
250.00	198.68	45.2441	0.0832	1.4938
300.00	218.66	45.1167	0.0908	1.6342
350.00	238.65	45.3460	0.1000	1.7913
400.00	258.66	46.0193	0.1115	1.9672
450.00	278.67	47.3751	0.1263	2.1657
500.00	298.69	49.8338	0.1468	2.3919
550.00	318.71	54.0581	0.1763	2.6491
600.00	338.74	61.7125	0.2238	2.9445

FIGURES

FIG. 1. Change in the band gap of $Hg_{0.78}Cd_{0.22}Te$ with temperature.

FIG. 2. Variation of conduction (dashed line) and valence (solid line) band edges of $Hg_{0.78}Cd_{0.22}Te$ with temperature.

FIG. 3. Derivative of direct gap with temperature for various semiconductor compounds and alloys as a function of zero-temperature gap. The vertical lines represent $Hg_{0.78}Cd_{0.22}Te$, InSb, InAs, $Hg_{0.5}Cd_{0.5}Te$, InP, GaAs and CdTe, respectively.

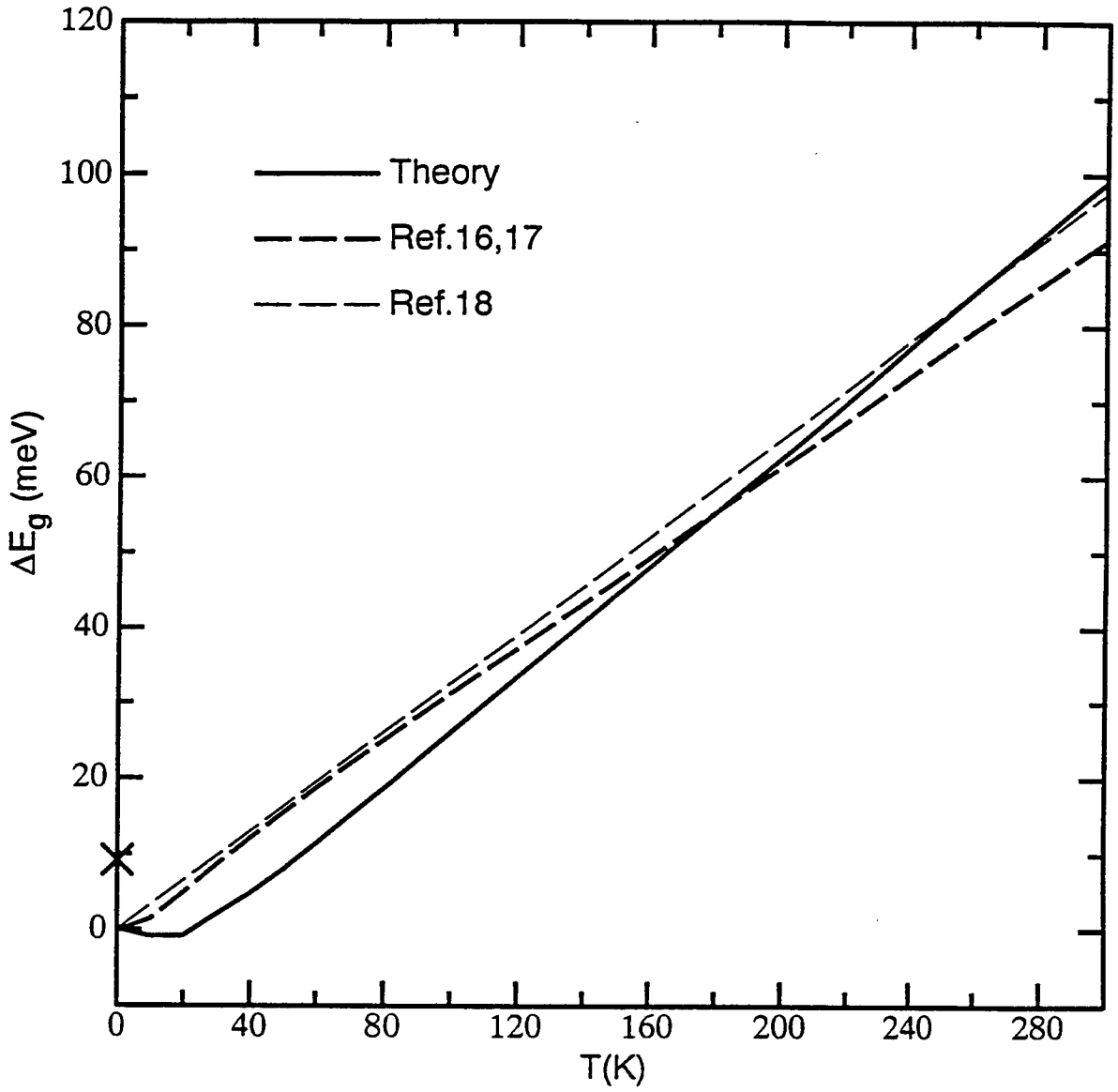
120
100
80
60
40
20
0
ΔE_g (meV)
Theory
Ref.16,17
Ref.18
0
40
80
120
160
200
240
280
T(K)

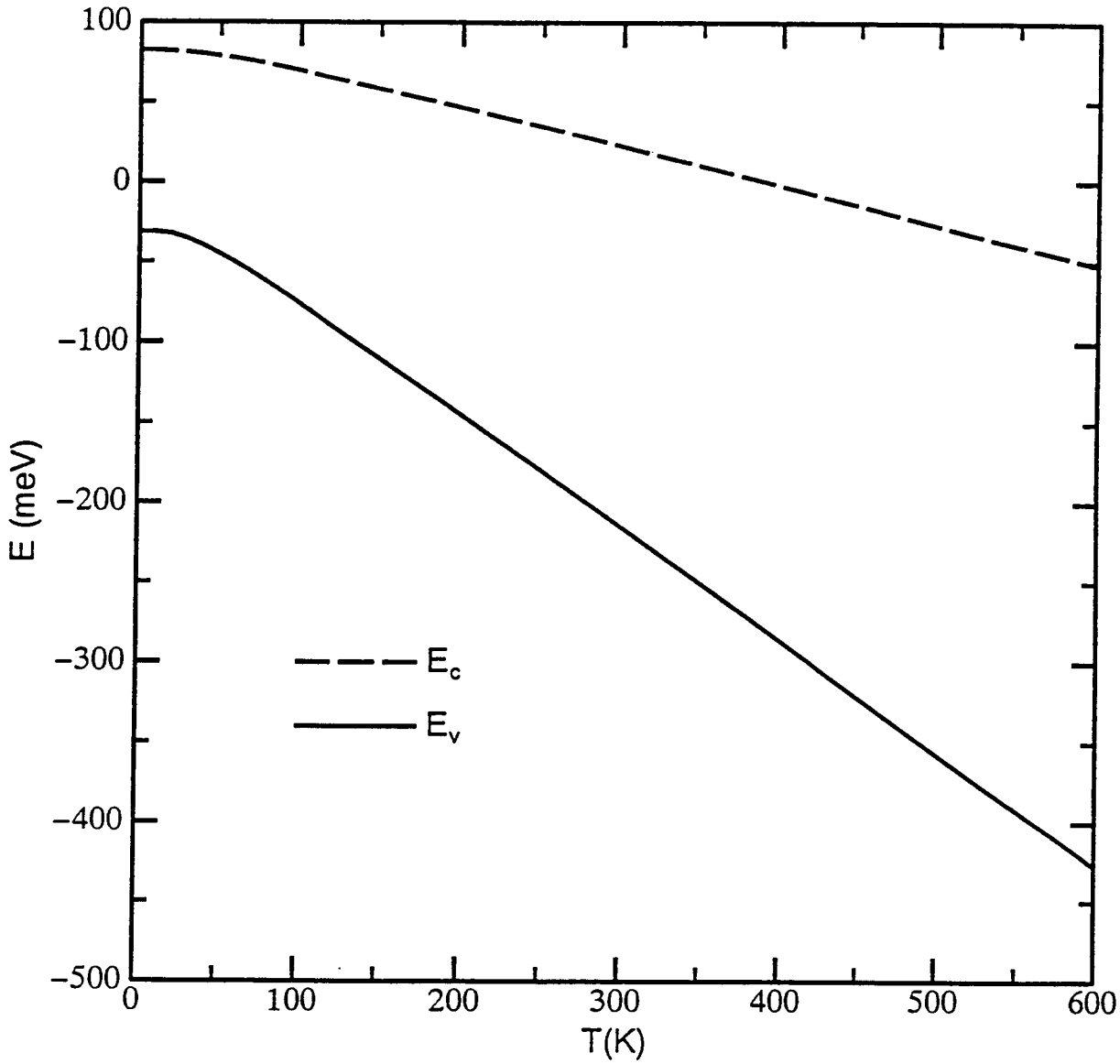
100
0
-100
-200
-300
-400
-500
E (meV)
0
100
200
300
400
500
600
T(K)
E_c
E_v

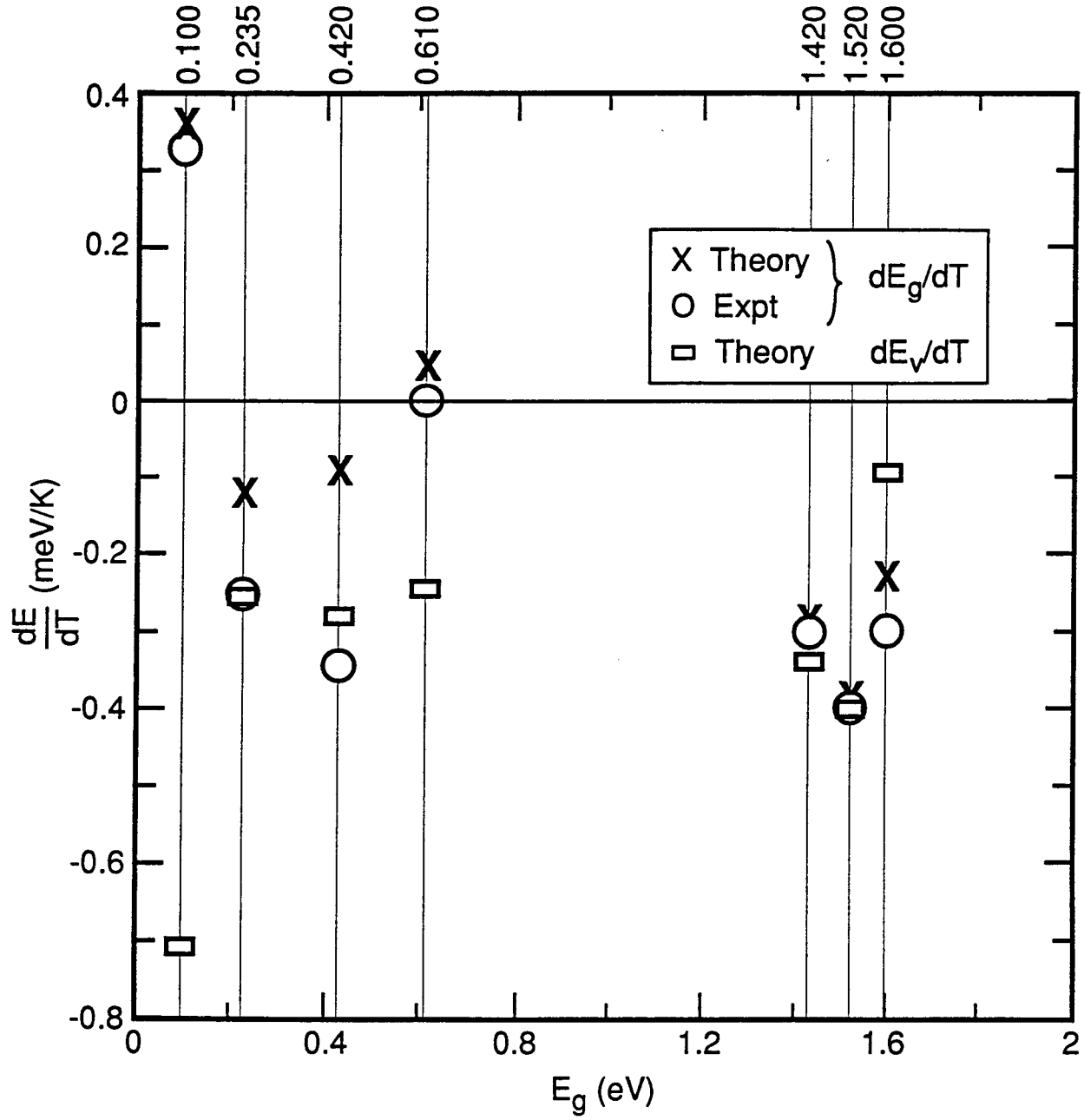
0.100
0.235
0.420
0.610
1.420
1.520
1.600
0.4
0.2
0
-0.2
-0.4
-0.6
-0.8
X Theory
O Expt
dEg/dT
Theory
dEv/dT
dE/dT (meV/K)
0
0.4
0.8
1.2
1.6
2
Eg (eV)